

Integrated Sensing and Communications in Downlink FDD MIMO without CSI Feedback

Namhyun Kim, Juntaek Han, Jinseok Choi, Ahmed Alkhateeb, Chan-Byoung Chae, and Jeonghun Park

Abstract—In this paper, we propose a precoding framework for frequency division duplex (FDD) integrated sensing and communication (ISAC) systems with multiple-input multiple-output (MIMO). Specifically, we aim to maximize ergodic sum spectral efficiency (SE) while satisfying a sensing beam pattern constraint defined by the mean squared error (MSE). Our method reconstructs downlink (DL) channel state information (CSI) from uplink (UL) training signals using partial reciprocity, eliminating the need for CSI feedback. To mitigate interference caused by imperfect DL CSI reconstruction and sensing operations, we adopt rate-splitting multiple access (RSMA). We observe that the error covariance matrix of the reconstructed channel effectively compensates for CSI imperfections, affecting both communication and sensing performance. To obtain this, we devise an *observed Fisher information*-based estimation technique. We then optimize the precoder by solving the Karush-Kuhn-Tucker (KKT) conditions, jointly updating the precoding vector and Lagrange multipliers, and solving the nonlinear eigenvalue problem with eigenvector dependency to maximize SE. The numerical results show that the proposed design achieves precise beam pattern control, maximizes SE, and significantly improves the sensing-communication trade-off compared to the state-of-the-art methods in FDD ISAC scenarios.

Index Terms—Integrated sensing and communications (ISAC), rate-splitting multiple access (RSMA), error covariance estimation, generalized power iteration (GPI).

I. INTRODUCTION

The convergence between wireless communication and sensing technologies is driving the development of innovative applications in next-generation networks, such as autonomous driving, smart cities, and environmental monitoring systems [1]–[3]. In this regard, the concept of integrated sensing and communication (ISAC) has been recognized as a vital approach, enabling simultaneous sensing and communication within a unified system architecture [1]. This method not only improves spectral efficiency (SE), but also significantly

This work was supported in part by Institute of Information & Communications Technology Planning & Evaluation (IITP) grant funded by the Korea government (MSIT) (No. RS-2024-00397216, Development of the Upper-mid Band Extreme massive MIMO (E-MIMO)), and in part by Institute of Information & Communications Technology Planning & Evaluation (IITP) grant funded by the Korea government (MSIT) (No. RS-2024-00428780, 6G-Cloud Research and Education Open Hub). Namhyun Kim, Juntaek Han, and Jeonghun Park are with the School of Electrical and Electronic Engineering, Yonsei University, Seoul 03722, South Korea (e-mail: namhyun@yonsei.ac.kr; jthan1218@yonsei.ac.kr; jhpark@yonsei.ac.kr). Jinseok Choi is with the School of Electrical Engineering, Korea Advanced Institute of Science and Technology (KAIST), Daejeon 34141, South Korea (e-mail: jinseok@kaist.ac.kr). Ahmed Alkhateeb is with the School of Electrical, Computer and Energy Engineering, Arizona State University, Tempe 85287, AZ, USA (e-mail: alkhateeb@asu.edu). C. B. Chae is with the School of Integrated Technology, Yonsei University, Seoul, 03722, South Korea (e-mail: cbchae@yonsei.ac.kr).

reduces hardware costs and energy consumption by sharing resources between sensing and communication [4], [5].

Integrating ISAC into current cellular systems requires a critical decision on the duplex mode, choosing between frequency division duplex (FDD) and time division duplex (TDD) [1], [5], [6]. Recent studies show that while TDD ISAC benefits from simplified channel estimation thanks to channel reciprocity, it may not be suitable for low-latency services due to the inherent delay caused by UE and BS having to wait for their respective transmission slots [5]–[7]. Additionally, TDD ISAC requires an extended guard interval to receive and process echo signals for target detection before uplink (UL) transmission, further increasing latency. This poses challenges for applications sensitive to delays, such as autonomous driving [5], [7]. As a remedy, FDD allows simultaneous UL and DL transmissions, eliminating the need for subframe switching and guard intervals. This underscores FDD’s importance for low-latency ISAC applications. The relationship between ISAC echo signals and UL communication signals for each duplex mode is shown in Fig. 1. Unfortunately, however, FDD still faces challenges due to the lack of channel reciprocity, which leads to substantial overhead in acquiring DL CSI for communication, which scales with the number of antennas and users [8], [9]. To address this, we propose a novel precoding framework that reconstructs DL CSI from UL training and enhances both communication and sensing capabilities.

A. Related Work

Early studies on the coexistence of communication and radar systems, which operated on separate hardware with shared spectrum [10], paved the way for the development of ISAC based on a unified infrastructure. In ISAC systems, maximizing efficiency requires the simultaneous support of multiple communication users and detection targets. This has driven research into MIMO-ISAC.

In the literature on MIMO-ISAC, the design of the transmit precoder has been a key topic. For example, [11] developed a branch-and-bound framework to achieve the global optimal solution that minimizes the mean square error (MSE) of the beam pattern under a constant modulus constraint. However, this approach does not assume designated radar symbols, making it sub-optimal compared to considering respective symbols for communication and sensing. To address this, a joint beamforming design for dedicated communication and sensing symbols was proposed in [3]. The authors in [12] introduced a generalized Pareto optimization framework,

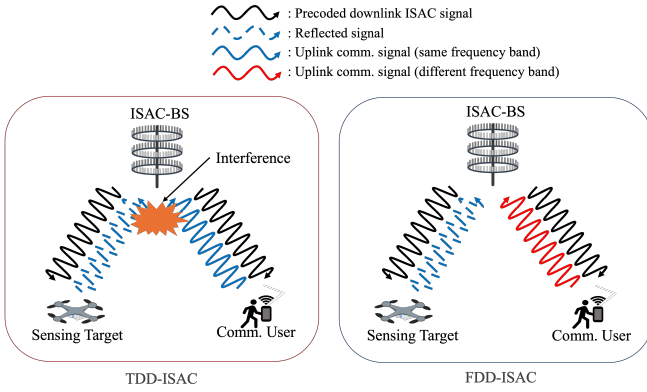


Fig. 1: While TDD ISAC, which uses the same bandwidth for DL and UL, requires a sufficient guard interval to separate the echo signal from the UL communication, FDD ISAC does not require a guard interval due to its separation in the frequency domain.

applying a bisection search algorithm to meet the lowest acceptable performance levels for dual functionalities. More recently, [4] proposed a rate-splitting multiple access (RSMA)-based precoder optimization technique to mitigate interference caused by added sensing functionality. However, the studies in [3], [4], [11], [12] did not account for the imperfections in CSI at the transmitter (CSIT), which are inevitable in practical wireless communication systems [13], [14].

In light of this, there have also been research endeavors that take into account CSIT imperfection. Specifically, in [15], channel estimation errors were addressed for MIMO-ISAC, whose key idea is minimizing the worst-cast multi-user interference. In [16], [17], robust beamforming designs for ISAC were proposed using techniques related to physical layer security or reconfigurable intelligent surface (RIS). In addition, robust ISAC beamforming methods for coping with CSIT imperfection were also investigated in [2], [16]–[18]. In this work, two types of CSIT error modeling were adopted:

Gaussian error with known covariance : The CSIT error is modeled as a Gaussian with known covariance [2], [16], [18]. This corresponds to FDD MIMO with scalar quantization.

Bounded error: The magnitude of the CSIT error is assumed to be bounded within certain ranges [15]–[17]. This corresponds to FDD MIMO with vector quantization.

In summary, the existing error modeling is established under the assumption of channel feedback in FDD MIMO systems. However, we recall that the amount of feedback often negates SE gains, as it scales with the number of antennas and users [8], [14], which fundamentally limits the potential gains of MIMO-ISAC; thus developing a low-complexity CSI acquisition approach is essential. To address this issue, in [19]–[22], the concept of eliminating CSI feedback was explored in FDD MIMO to simplify the CSI acquisition process, known as zero-feedback strategies. A key idea of the zero-feedback strategy is to leverage partial channel reciprocity to efficiently reconstruct the DL channel from UL reference signals, by which we can omit the direct channel feedback

even in FDD. However, with these DL CSIT reconstruction approaches, the CSIT error cannot be avoided due to the discrepancies between the UL and DL environments [20]. Unfortunately, it is not feasible to employ the previous CSIT error treatment approaches to handle the CSIT error caused by zero-feedback strategies [20], [22]. That is to say, it is reasonable to assume that the corresponding CSIT error is *not bounded* as in [15]–[17] since CSI quantization is not used in zero-feedback strategies. Further, *its error covariance cannot be obtained* in a straightforward way because highly nonlinear algorithms are typically used to reconstruct the DL CSIT from UL reference signals such as [23]. To resolve this, there have been attempts to approximate the CSIT error covariance using the Cramér-Rao lower bound matrix (CRLB) [22], [24]. Specifically, in [24], they computed the CRLB matrix in an instantaneous manner during UL training. Incorporating this into the precoder design, it was found that significant SE gains could be achieved even without CSI feedback in FDD MIMO. Consequently, it is promising to explore the zero-feedback strategy for MIMO-ISAC.

B. Contributions

In this paper, we present a novel FDD MIMO-ISAC transmission framework that does not necessitate CSI feedback. Unlike a conventional approach, we reconstruct the DL CSI solely based on UL sounding reference signals by following [21], [24]. In this setup, acquiring perfect DL CSIT is infeasible, making efficient mitigation of interference arising from imperfect DL CSIT crucial to achieve robust SE and ensure sensing performance. In this perspective, we summarize our main contributions as follows.

- We investigate a DL channel reconstruction method in which channel parameters are estimated solely from UL training. The main problem is then formulated to maximize the sum SE under imperfect CSIT while meeting a beam pattern matching constraint based on a target MSE. To address CSIT inaccuracies caused by zero feedback, we consider the RSMA technique. The communication rate for the common message is defined using a minimum function to ensure that it is decodable by all users. For the sensing constraint, we represent the MSE between the desired and actual beam pattern in a quadratic form. In solving the formulated problem, we find that accurate CSI error covariance matrix estimation is crucial to designing precoders that effectively cope with CSIT inaccuracies.
- To obtain the error covariance matrix, we propose a novel method, assuming partial reciprocity in the given channel model. In particular, we note that the MSE of the UL channel estimated with the 2D-NOMP estimator closely approaches the CRLB level as demonstrated in [21]. Based on this, we estimate the error covariance matrix by evaluating the CRLB using the UL received signal. Specifically, we exploit the observed Fisher information, which effectively estimates the realized error when only the *estimated* channel parameter is available. We highlight that the proposed method can effectively provide robustness in the absence of direct CSI feedback.

- To solve the formulated problem, we provide an efficient precoding method inspired by the KKT (Karush-Kuhn-Tucker) conditions, which alternately optimizes the precoding vector and the Lagrange multiplier to satisfy the KKT conditions without the need for any off-the-shelf optimization tools. Specifically, we use the principle of nonlinear eigenvalue problem with eigenvector dependency (NEPv) [25] for designing the precoding vectors. We also find that the Lagrange multiplier dictates the design orientation between sensing and communication, which implies the versatility of the proposed method.

Our approach is particularly advantageous in that it achieves robust SE and also precise sensing performance in FDD MIMO systems, all while eliminating the need for CSI feedback. Through this, we provide valuable design insights for FDD MIMO-ISAC systems with low overhead.

Notation: The superscripts $(\cdot)^T$, $(\cdot)^H$, $(\cdot)^{-1}$, $(\cdot)^\dagger$ denote the transpose, Hermitian, matrix inversion, and Moore-Penrose pseudo-inverse, respectively. \mathbf{I}_N is the identity matrix of size $N \times N$. Assuming that $\mathbf{A}_1, \dots, \mathbf{A}_N \in \mathbb{C}^{K \times K}$, $\mathbf{A} = \text{blkdiag}(\mathbf{A}_1, \dots, \mathbf{A}_n, \dots, \mathbf{A}_N)$ is a block-diagonal matrix concatenating $\mathbf{A}_1, \dots, \mathbf{A}_N$. We use $\lfloor \cdot \rfloor$, $\lceil \cdot \rceil$ to denote the rounding of a decimal number to its nearest lower and higher integers, respectively. $\mathbf{A} \circ \mathbf{B}$ denotes the Hadamard product of the two matrices \mathbf{A} and \mathbf{B} . $[K]$ is the set of natural numbers less than or equal to K .

II. SYSTEM MODEL

In this section, we describe the UL and DL channel model and introduce the ISAC signal model assisted by RSMA.

A. Communication Channel Model

Consider a MIMO system with orthogonal frequency division multiplexing (OFDM), in which a base station (BS) has a uniform linear array (ULA) consisting of N antennas and each user is equipped with a single antenna. We assume that there are a total of S pilots for the UL band, with their frequency spacing denoted as Δf , which implicitly represents the bandwidth of each coherence block. The total bandwidth is set as $B = S\Delta f$. Adopting the multipath model used in [19], [21], we represent the narrowband baseband UL channel from user k to n -th BS antenna over the s -th sub-carrier ($k \in [K], n \in [N]$ and $s \in [S]$) as follows:

$$h_{k,n,s}^{\text{ul}} = \sum_{\ell=1}^{L_k^{\text{ul}}} \alpha_{k,\ell}^{\text{ul}} e^{-j2\pi(n-1)\phi_{k,\ell,s}^{\text{ul}}} e^{-j2\pi(s-\lceil \frac{S}{2} \rceil - 1)\Delta f \tau_{k,\ell}^{\text{ul}}}, \quad (1)$$

assuming half wavelength array spacing, $\phi_{k,\ell,s}^{\text{ul}}$ is given by

$$\phi_{k,\ell,s}^{\text{ul}} = \frac{\sin \theta_{k,\ell}}{2} \left(1 + \frac{s\Delta f}{f_c^{\text{ul}}} \right), \quad (2)$$

and $\alpha_{k,\ell}^{\text{ul}} \in \mathbb{C}^{1 \times 1}$, $\tau_{k,\ell}^{\text{ul}} \in \mathbb{R}^{1 \times 1}$ denote the complex path gain and propagation delay of the ℓ -th path for user k respectively. Both are assumed to be consistent in entire bandwidth for UL [21], [26]. We assume that the propagation delay is given by $0 < \tau_{k,\ell}^{\text{ul}} < 1/\Delta f$, and the number of paths as L_k^{ul} . The AoA of ℓ -th path for user k is denoted as $\theta_{k,\ell}^{\text{ul}}$, the wavelength of

UL carrier frequency as λ_c^{ul} , and the antenna spacing for UL reception as d^{ul} with $d^{\text{ul}} = \lambda_c^{\text{ul}}/2$. Similarly, the DL channel from n -th BS antenna to user k over the s -th sub-carrier of DL channel is expressed as

$$h_{k,n,s}^{\text{dl}}(f) = \sum_{\ell=1}^{L_k^{\text{dl}}} \alpha_{k,\ell}^{\text{dl}} e^{-j2\pi(n-1)\phi_{k,\ell,s}^{\text{dl}}} e^{-j2\pi(f+(s-\lceil \frac{S}{2} \rceil - 1)\Delta f)\tau_{k,\ell}^{\text{dl}}}, \quad (3)$$

in which we assume that f denotes the frequency difference between carrier frequency of UL and DL, and the DL parameters such as $L_k^{\text{dl}}, \alpha_{k,\ell}^{\text{dl}}, \phi_{k,\ell,s}^{\text{dl}}, \theta_{k,\ell}^{\text{dl}}, \tau_{k,\ell}^{\text{dl}}$ is defined in the same manner as UL. As reported in numerous previous studies with actual measurements [19], [21], the UL and DL channels share the following parameters:

- **Propagation delay:** $\tau_{k,\ell}^{\text{ul}} = \tau_{k,\ell}^{\text{dl}}$.
- **Angular parameter:** $\theta_{k,\ell}^{\text{ul}} = \theta_{k,\ell}^{\text{dl}}$.
- **Channel path number:** $L_k^{\text{ul}} = L_k^{\text{dl}} \triangleq L_k$.

However, channel gains may not exhibit perfect reciprocity [21], [27]. To account for this, we model the DL channel gain as

$$\alpha_{k,\ell}^{\text{dl}} = \eta_{k,\ell} \alpha_{k,\ell}^{\text{ul}} + \sqrt{1 - \eta_{k,\ell}^2} \beta_{k,\ell}, \quad (4)$$

where $\beta_{k,\ell}$ is assumed to be a random variable following $\mathcal{CN}(0, \sigma_{\text{path},k,\ell}^2)$, $\forall \ell$, independent of the UL channel gain $\alpha_{k,\ell}^{\text{ul}}$. In the special case where $\eta_{k,\ell} = 1, \forall (k, \ell)$, our model reduces to a reciprocal channel gain case ($\alpha_{k,\ell}^{\text{dl}} = \alpha_{k,\ell}^{\text{ul}}$) considered in the previous work [19], [26], and therefore we consider a more generalized scenario.

B. RSMA-assisted MIMO-ISAC Signal Model

In this study, we anticipate that the unified hardware structure for ISAC may lead to a lack of available spatial resources. To effectively address this, we consider RSMA, a multiple access technique that enhances robustness when spatial resources are shared for multiple objectives [28]. Specifically, RSMA mitigates interference between sensing and communication, as well as among communication users [4], [25], [29]. In RSMA, each user's message M_k is split into a common part $M_{c,k}$ and a private part $M_{p,k}$. The common parts are encoded into a single common stream s_c , while private parts are encoded individually as $s_k, k \in [K]$. At the receiver, each user k first decodes the common stream, removes it using successive interference cancellation (SIC), and then decodes the private stream s_k while treating residual interference as noise [28].

To fully exploit the spatial degrees of freedom (DoF) available in the considered MIMO system, the BS uses dedicated radar signals combined with communication symbols for transmission. Accordingly, the transmitted signal, denoted as $\mathbf{x} \in \mathbb{C}^N$, is given as

$$\begin{aligned} \mathbf{x} &= \mathbf{p}_c s_c + \mathbf{P}_p \mathbf{s}_p + \mathbf{P}_r \mathbf{s}_r \\ &= [\mathbf{P}_c, \mathbf{P}_r] [\mathbf{s}_c^T, \mathbf{s}_r^T]^T = \mathbf{P} \mathbf{s}, \end{aligned} \quad (5)$$

where \mathbf{p}_c denotes the precoding vector for the common message symbol s_c , \mathbf{P}_p is a precoding matrix for private message vector $\mathbf{s}_p = [s_{p,1}, s_{p,2}, \dots, s_{p,K}]^T$, which is defined as $\mathbf{P}_p =$

$\{\mathbf{p}_{p,1}, \mathbf{p}_{p,2}, \dots, \mathbf{p}_{p,K}\} \in \mathbb{C}^{N \times K}$, where $\mathbf{p}_{p,k}$ is the precoder for the private message of user k . Likewise, \mathbf{P}_r represents the precoding matrix for the vector of radar sequence symbols $\mathbf{s}_r = [s_{r,1}, s_{r,2}, \dots, s_{r,M}]^T$, that is, $\mathbf{P}_r = [\mathbf{p}_{r,1}, \mathbf{p}_{r,2}, \dots, \mathbf{p}_{r,M}] \in \mathbb{C}^{N \times M}$, where $\mathbf{p}_{p,m}$ is the radar beamformer for the m -th radar symbol. For notational simplicity, we integrate the common and private part with a single expression, which is given by $\mathbf{P}_c = [\mathbf{p}_c, \mathbf{P}_p]$ and $\mathbf{s}_c = [s_c, \mathbf{s}_p^T]^T$. Lastly, we define the entire precoding vector and the symbol vector as $\mathbf{P} = [\mathbf{P}_c, \mathbf{P}_r]$ and $\mathbf{s} = [\mathbf{s}_c^T, \mathbf{s}_r^T]^T$, respectively. The communication symbols \mathbf{s}_c and the radar sequences \mathbf{s}_r are statistically independent of each other [2], that is, $\mathbb{E}[\mathbf{s}_c \mathbf{s}_r^H] = \mathbf{0}_{(K+1) \times M}$. In addition, the power constraint with transmit power P is represented by $\mathbb{E}[\mathbf{s}_c \mathbf{s}_c^H] = P \cdot \mathbf{I}_{K+1}$ and $\mathbb{E}[\mathbf{s}_r \mathbf{s}_r^H] = P \cdot \mathbf{I}_M$, respectively. In this regard, we presume that $\|\mathbf{P}_c\|_F + \|\mathbf{P}_r\|_F \leq 1$, without loss of generality.

III. DOWNLINK CHANNEL RECONSTRUCTION & PERFORMANCE METRICS

In this section, we explore a DL channel reconstruction method based on UL training and define performance metrics for communication and sensing, respectively.

A. Reconstructing the Downlink Channel

We start by introducing the vector $\mathbf{u}(\tau_{k,\ell}, \theta_{k,\ell}) \in \mathbb{C}^{NS \times 1}$ which encapsulates the spatial signature along with the delay profile for each sub-carrier. The specific element corresponding to the n -th antenna and the s -th sub-carrier is

$$[\mathbf{u}(\tau_{k,\ell}, \theta_{k,\ell})]_{n,s} = e^{-j2\pi(n-1)\phi_{k,\ell,s}^{\text{ul}}} e^{-j2\pi(s - \lceil \frac{S}{2} \rceil - 1)\Delta f \tau_{k,\ell}^{\text{ul}}}, \quad (6)$$

which comes from the channel model in (1).

Assuming that the UL sounding reference signal comprises ones for all sub-carriers and antennas without loss of generality, the received signal vector $\mathbf{y}_k \in \mathbb{C}^{NS \times 1}$ that represents the signals across all antennas and sub-carriers is described by

$$\mathbf{y}_k = \sum_{\ell=1}^{L_k} \alpha_{k,\ell}^{\text{ul}} \mathbf{u}(\tau_{k,\ell}, \theta_{k,\ell}) + \mathbf{n}_k, \quad (7)$$

where $\mathbf{n}_k \in \mathbb{C}^{NS \times 1}$ follows the additive white Gaussian noise (AWGN). Our aim is to estimate the DL channel from the UL-observed signal \mathbf{y}_k . To achieve this, we first identify the set of parameters of the UL channel $\{\hat{\alpha}_{k,\ell}^{\text{ul}}, \hat{\tau}_{k,\ell}^{\text{ul}}, \hat{\theta}_{k,\ell}^{\text{ul}}\}_{\ell=1, \dots, L_k}$ from \mathbf{y}_k , then reconstruct the DL channel at the frequency difference f by exploiting their frequency invariance discussed in Section II.

For this task, we employ the 2D-NOMP algorithm, which is a state-of-the-art compressed sensing method [21], [23]. This approach is particularly useful, as it circumvents the need for knowledge of number of channel paths while operating efficiently in a grid-less context. Its effectiveness has been validated in practical settings, as demonstrated in [21]. The detailed procedure of the 2D-NOMP algorithm is elaborated in [21], [24]; and we omit it in this paper to conserve space.

As the output, we obtain the quadruplets of estimated UL parameters with $\hat{\alpha}_{k,\ell}^{\text{ul}} = \Re\{\hat{\alpha}_{k,\ell}^{\text{ul}}\} + j\Im\{\hat{\alpha}_{k,\ell}^{\text{ul}}\}$ i.e.,

$$\hat{\mathcal{P}}_k = \left\{ \Re\{\hat{\alpha}_{k,\ell}^{\text{ul}}\}, \Im\{\hat{\alpha}_{k,\ell}^{\text{ul}}\}, \hat{\tau}_{k,\ell}^{\text{ul}}, \hat{\theta}_{k,\ell}^{\text{ul}} \right\}_{\ell=1, \dots, L_k}, \quad (8)$$

they are used to estimate the DL channel parameters $\{\hat{\alpha}_{k,\ell}^{\text{dl}}, \hat{\tau}_{k,\ell}^{\text{dl}}, \hat{\theta}_{k,\ell}^{\text{dl}}\}_{\ell=1, \dots, L_k}$, considering the frequency invariance property. Taking the randomness of channel gain in (4) into account, we determine the estimated channel parameter for DL as

$$\left\{ \hat{\alpha}_{k,\ell}^{\text{dl}}, \hat{\tau}_{k,\ell}^{\text{dl}}, \hat{\theta}_{k,\ell}^{\text{dl}} \right\} \triangleq \left\{ \eta_{k,\ell} \hat{\alpha}_{k,\ell}^{\text{ul}}, \hat{\tau}_{k,\ell}^{\text{ul}}, \hat{\theta}_{k,\ell}^{\text{ul}} \right\}, \forall (k, \ell). \quad (9)$$

With this, we can reconstruct the DL channel in (3), which is represented by

$$\hat{h}_{k,n,s}^{\text{dl}}(f) = \sum_{\ell=1}^{L_k^{\text{dl}}} \hat{\alpha}_{k,\ell}^{\text{dl}} e^{-j2\pi(n-1)\hat{\phi}_{k,\ell,s}^{\text{dl}}} e^{-j2\pi(f + (s - \lceil \frac{S}{2} \rceil - 1)\Delta f)\hat{\tau}_{k,\ell}^{\text{dl}}}, \quad (10)$$

where $\hat{\phi}_{k,\ell,s}^{\text{ul}}$ is defined as

$$\hat{\phi}_{k,\ell,s}^{\text{ul}} = \frac{\sin \hat{\theta}_{k,\ell}}{2} \left(1 + \frac{s\Delta f}{f_c} \right). \quad (11)$$

Correspondingly, the spatial reconstructed channel of (narrow-band) s -th resource block at f for user k is defined as

$$\hat{\mathbf{h}}_{k,s}(f) = [\hat{h}_{k,1,s}^{\text{dl}}(f), \hat{h}_{k,2,s}^{\text{dl}}(f), \dots, \hat{h}_{k,N,s}^{\text{dl}}(f)] \in \mathbb{C}^{N \times 1}. \quad (12)$$

For notational simplicity, our signal model and performance metrics that we will find later omit the subcarrier index s and the extrapolation range f , assuming that our interested narrow-band DL channel is fixed. Thus, $\hat{\mathbf{h}}_{k,s}(f)$ and its ground truth $\mathbf{h}_{k,s}(f)$ will be simply referred to as $\hat{\mathbf{h}}_k$ and \mathbf{h}_k , respectively.

B. Communication & Sensing Performance Metric

In this subsection, we aim to characterize the communication performance metric given the imperfect CSIT, and also to define the sensing performance metric for the design of the beam pattern.

1) *Communication Performance Metric*: We consider the ergodic sum SE as the communication performance metric. To investigate this, we first represent the received signal at user k , denoted as y_k , as follows:

$$y_k = \mathbf{h}_k^H \mathbf{p}_c s_c + \sum_{i=1}^K \mathbf{h}_k^H \mathbf{p}_{p,i} s_{p,i} + \sum_{m=1}^M \mathbf{h}_k^H \mathbf{p}_{r,m} s_{r,m} + z_k, \quad (13)$$

where $z_k \sim \mathcal{CN}(0, \sigma^2)$ follows AWGN. With this signal model, we aim to maximize the ergodic sum SE under imperfect CSIT. Given that the channel estimate $\hat{\mathbf{h}}_k$ is provided, the instantaneous SE for the common and private messages is defined as the expectation over the CSIT error \mathbf{e}_k :

$$R_{c,k}^i(\mathbf{P}) = \mathbb{E}_{\mathbf{e}_k} \left[\log_2 \left(\frac{|\mathbf{h}_k^H \mathbf{p}_c|^2}{\sum_{i=1}^K |\mathbf{h}_k^H \mathbf{p}_{p,i}|^2 + \sigma^2/P} \right) \middle| \hat{\mathbf{h}}_k \right], \quad (14)$$

$$R_{p,k}^i(\mathbf{P}) = \mathbb{E}_{\mathbf{e}_k} \left[\log_2 \left(\frac{|\mathbf{h}_k^H \mathbf{p}_{p,k}|^2}{\sum_{i=1, i \neq k}^K |\mathbf{h}_k^H \mathbf{p}_{p,i}|^2 + \sigma^2/P} \right) \middle| \hat{\mathbf{h}}_k \right]. \quad (15)$$

The instantaneous rate of the common message s_c is set to ensure decodability for all users, i.e.,

$$R_c^i(\mathbf{P}) = \min_{k \in [K]} R_{c,k}^i(\mathbf{P}). \quad (16)$$

Note, however, that the expressions in (14), (15) are not in closed form as they are represented with the expectation. To use them as an objective function for our problem, it is required to develop this into a tractable representation. Accordingly, using the direct relationship $\mathbf{h}_k = \hat{\mathbf{h}}_k + \mathbf{e}_k$, the received signal in (13) is represented by

$$y_k = \hat{\mathbf{h}}_k^H \mathbf{p}_c s_c + \underbrace{\sum_{i=1}^K \hat{\mathbf{h}}_k^H \mathbf{p}_{p,i} s_{p,i} + \sum_{m=1}^M \hat{\mathbf{h}}_k^H \mathbf{p}_{r,m} s_{r,m}}_{(a)} + \underbrace{\mathbf{e}_k^H \mathbf{p}_c s_c + \sum_{i=1}^K \mathbf{e}_k^H \mathbf{p}_{p,i} s_{p,i} + \sum_{m=1}^M \mathbf{e}_k^H \mathbf{p}_{r,m} s_{r,m} + z_k}_{(a)}. \quad (17)$$

Treating each term in (a) as independent Gaussian noise, the average received signal power at user k , normalized by P given the channel state, is denoted as follows:

$$\begin{aligned} & \frac{\mathbb{E}\{|y_k|^2\}}{P} \\ &= \underbrace{|\hat{\mathbf{h}}_k^H \mathbf{p}_c|^2}_{S_{c,k}} + \underbrace{|\hat{\mathbf{h}}_k^H \mathbf{p}_{p,k}|^2}_{S_k} + \underbrace{\sum_{i=1, i \neq k}^K |\hat{\mathbf{h}}_k^H \mathbf{p}_{p,i}|^2 + \sum_{m=1}^M |\hat{\mathbf{h}}_k^H \mathbf{p}_{r,m}|^2}_{I_{c,k}} \\ & \quad + \underbrace{|\mathbf{e}_k^H \mathbf{p}_c|^2 + \sum_{i=1}^K |\mathbf{e}_k^H \mathbf{p}_{p,i}|^2 + \sum_{m=1}^M |\mathbf{e}_k^H \mathbf{p}_{r,m}|^2 + \frac{\sigma^2}{P}}_{I_{c,k}}, \end{aligned} \quad (18)$$

where we indicate the power of the desired signal in the common part as $S_{c,k}$ and in the private part as S_k , and the corresponding interference as $I_{c,k}$ and I_k , respectively. In fact, the independent Gaussian noise assumption suggests the worst case of mutual information to derive a lower bound of (14), (15) [25]. Specifically, a lower bound of instantaneous SE for the common message is further derived as

$$\begin{aligned} R_{c,k}^i(\mathbf{P}) &\geq \mathbb{E}_{\mathbf{e}_k} [\log_2(1 + S_{c,k} I_{c,k}^{-1})] \quad (19) \\ &\stackrel{(a)}{\geq} \log_2 \left(1 + \frac{|\hat{\mathbf{h}}_k^H \mathbf{p}_c|^2}{\left\{ \sum_{i=1}^K |\hat{\mathbf{h}}_k^H \mathbf{p}_{p,i}|^2 + \sum_{i=1}^K \mathbf{p}_{p,i}^H \mathbb{E}[\mathbf{e}_k \mathbf{e}_k^H] \mathbf{p}_{p,i} \right.} \right. \\ & \quad \left. \left. + \sum_{m=1}^M |\hat{\mathbf{h}}_k^H \mathbf{p}_{r,m}|^2 + \sum_{m=1}^M \mathbf{p}_{r,m}^H \mathbb{E}[\mathbf{e}_k \mathbf{e}_k^H] \mathbf{p}_{r,m} + \frac{\sigma^2}{P} \right\}} \right) \quad (20) \\ &\stackrel{(b)}{=} \log_2 \left(1 + \frac{|\hat{\mathbf{h}}_k^H \mathbf{p}_c|^2}{\left\{ \sum_{p=1}^K |\hat{\mathbf{h}}_k^H \mathbf{p}_{p,i}|^2 + \sum_{m=1}^M |\hat{\mathbf{h}}_k^H \mathbf{p}_{r,m}|^2 \right.} \right. \\ & \quad \left. \left. + \sum_{p=1}^K \mathbf{p}_{p,i}^H \Sigma_k \mathbf{p}_{p,i} + \sum_{m=1}^M \mathbf{p}_{r,m}^H \Sigma_k \mathbf{p}_{r,m} + \frac{\sigma^2}{P} \right\}} \right) \quad (21) \\ &\triangleq \bar{R}_{c,k}^i(\mathbf{P}). \end{aligned}$$

We note that the inequality (a) follows from the Jensen's inequality, i.e., $\mathbb{E}[\log_2(1 + 1/x)] \geq \log_2(1 + 1/\mathbb{E}[x])$, where we omit the subscript of \mathbf{e}_k due to the space limitation. (b) comes from $\mathbb{E}[\mathbf{e}_k \mathbf{e}_k^H] = \Sigma_k$. Similar to (16), we can define a lower bound for the instantaneous rate of common message as well, i.e.,

$$\bar{R}_c^i(\mathbf{P}) = \min_{k \in [K]} \bar{R}_{c,k}^i(\mathbf{P}). \quad (22)$$

Recall that our objective is to maximize the ergodic sum SE. Considering multiple fading processes, the ergodic SE of the common message is determined as

$$R_c = \min_{k \in \mathcal{K}} \left\{ \mathbb{E}_{\hat{\mathbf{h}}_k} [R_{c,k}^i(\mathbf{P})] \right\} \geq \min_{k \in \mathcal{K}} \left\{ \mathbb{E}_{\hat{\mathbf{h}}_k} [\bar{R}_{c,k}^i(\mathbf{P})] \right\} \geq \mathbb{E}_{\hat{\mathbf{h}}_k} [\bar{R}_c^i(\mathbf{P})]. \quad (23)$$

Notably, we will use (23) as our objective function to maximize the ergodic rate of the common message, which corresponds to maximizing the lower bound in (22) for each fading block. Similarly, a lower bound for the instantaneous SE of the private message is represented as

$$R_k^i(\mathbf{P}) \geq \mathbb{E}_{\mathbf{e}_k} [\log_2(1 + S_k I_k^{-1})], \quad (24)$$

$$\geq \log_2 \left(1 + \frac{|\hat{\mathbf{h}}_k^H \mathbf{p}_{p,k}|^2}{\left\{ \sum_{i=1, i \neq k}^K |\hat{\mathbf{h}}_k^H \mathbf{p}_{p,i}|^2 + \sum_{i=1}^K \mathbf{p}_{p,i}^H \Sigma_k \mathbf{p}_{p,i} \right.} \right. \\ \left. \left. + \sum_{m=1}^M |\hat{\mathbf{h}}_k^H \mathbf{p}_{r,m}|^2 + \sum_{m=1}^M \mathbf{p}_{r,m}^H \Sigma_k \mathbf{p}_{r,m} + \frac{\sigma^2}{P} \right\}} \right) \quad (25)$$

$$\triangleq \bar{R}_k^i(\mathbf{P}), \quad (26)$$

which is also connected to its ergodic SE as

$$R_k = \mathbb{E}_{\hat{\mathbf{h}}_k} [R_k^i(\mathbf{P})] \geq \mathbb{E}_{\hat{\mathbf{h}}_k} [\bar{R}_k^i(\mathbf{P})]. \quad (27)$$

From (23) and (27), we derive the following lower bound on the ergodic sum SE, i.e., $R_\Sigma := R_c + \sum_{k=1}^K R_k$. That is,

$$R_\Sigma \geq \bar{R}_\Sigma = \mathbb{E}_{\hat{\mathbf{h}}_k} \left[\bar{R}_c^i(\mathbf{P}) + \sum_{k=1}^K \bar{R}_k^i(\mathbf{P}) \right]. \quad (28)$$

To maximize R_Σ , we use \bar{R}_Σ as a surrogate objective.

2) *Sensing Performance Metric*: As a sensing performance metric, we consider the MSE between the target beam pattern and the actual beam pattern. It should be noted that the MSE metric offers versatility, enabling features such as adaptive sensing beam widening to address angle uncertainties [2], [3], [30]. Comparisons of MSE and other possible sensing metrics such as CRLB [31] and SCNR (signal to clutter and noise ratio) are presented in [2].

Meanwhile, notice that we have two types of symbols, \mathbf{s}_c and \mathbf{s}_r , both of which are precoded to be transmitted as \mathbf{x} . Then we define the baseband narrowband signal in the direction of θ as

$$q(\theta) = \mathbf{a}^H(\theta) \mathbf{x}. \quad (29)$$

Using this, the average signal power for radar toward the direction θ is represented by

$$G(\mathbf{P}; \theta) = \mathbb{E}[|q(\theta)|^2] = P \cdot \mathbf{a}^H(\theta) \mathbf{P} \mathbf{a}(\theta). \quad (30)$$

We then compare this with the normalized target beam pattern $t(\theta_u)$ to define the sensing beam pattern MSE. Specifically, assuming L grids, where the detection angle θ_u is evenly sampled into L points, the MSE is defined as

$$\text{MSE}_r = \frac{1}{L} \sum_{u=1}^L |G(\mathbf{P}; \theta_u) - P \cdot t(\theta_u)|^2. \quad (31)$$

With this, we can also easily design sensing beams with multiple target angles by simply letting the target beam pattern for the desired direction as 1, i.e., $t(\theta_u) = 1$ otherwise as 0, i.e., $t(\theta_u) = 0$.

C. Problem Formulation

Note that maximizing the ergodic sum SE under the target radar beam pattern MSE T_{mse} is our main design objective. To achieve this, we aim to maximize the instantaneous achievable SE for each fading block [29] and formulate this as \mathcal{P}_0 :

$$\mathcal{P}_0 : \underset{\mathbf{P}}{\text{maximize}} \quad \min_{k \in [K]} R_{c,k}^i(\mathbf{P}) + \sum_{k=1}^K R_k^i(\mathbf{P}) \quad (32)$$

$$\text{subject to } \text{MSE}_r \leq T_{\text{mse}}, \quad (33)$$

$$\|\mathbf{P}\|_{\text{F}}^2 \leq 1. \quad (34)$$

As previously discussed, with the power constraint on the transmitted symbols $\mathbf{s} = [\mathbf{s}_c^T, \mathbf{s}_r^T]^T$ given by the budget P , the precoder norm is constrained to 1.

D. Problem Reformulation

1) *Problem Reformulation:* For the problem \mathcal{P}_0 , we notice that the expression in (32) is not a tractable form. To address this, we use a lower bound derived in the previous section, characterized in (22), (28) to maximize the instantaneous SE for each fading block. In addition, considering that the sum SE increases with transmit power [25], we just assume $\|\mathbf{P}\|_{\text{F}}^2 = 1$. Consequently, the reformulated problem is as follows:

$$\mathcal{P}_1 : \underset{\mathbf{P}}{\text{maximize}} \quad \min_{k \in [K]} \bar{R}_{c,k}^i(\mathbf{P}) + \sum_{k=1}^K \bar{R}_k^i(\mathbf{P}) \quad (35)$$

$$\text{subject to } \text{MSE}_r \leq T_{\text{mse}}, \quad (36)$$

$$\|\mathbf{P}\|_{\text{F}}^2 = 1. \quad (37)$$

Now, we rewrite the precoding matrix in vector form, that is, $\bar{\mathbf{p}} = \text{vec}(\mathbf{P}) \in \mathbb{C}^{N(K+M+1)}$, and $\|\bar{\mathbf{p}}\|^2 = 1$. By replacing \mathbf{P} with $\bar{\mathbf{p}}$, the SINR terms for the common message of user k in (21) and the private message of user k in (25) are reformulated into a tractable form, denoted as $\gamma_c(k)$ and γ_k , respectively, as follows:

$$\gamma_c(k) = \frac{\bar{\mathbf{p}}^H \mathbf{U}_c(k) \bar{\mathbf{p}}}{\bar{\mathbf{p}}^H \mathbf{V}_c(k) \bar{\mathbf{p}}}, \quad (38)$$

$$\gamma_k = \frac{\bar{\mathbf{p}}^H \mathbf{U}_k \bar{\mathbf{p}}}{\bar{\mathbf{p}}^H \mathbf{V}_k \bar{\mathbf{p}}}, \quad (39)$$

where

$$\mathbf{U}_c(k) = \text{blkdiag}((\hat{\mathbf{h}}_k \hat{\mathbf{h}}_k^H + \boldsymbol{\Sigma}_k), \dots, (\hat{\mathbf{h}}_k \hat{\mathbf{h}}_k^H + \boldsymbol{\Sigma}_k)) + \frac{\sigma^2}{P} \mathbf{I}_{N(K+M+1)}, \quad (40)$$

$$\mathbf{V}_c(k) = \mathbf{U}_c(k) - \text{blkdiag}(\hat{\mathbf{h}}_k \hat{\mathbf{h}}_k^H, \mathbf{0}, \dots, \mathbf{0}), \quad (41)$$

$$\mathbf{U}_k = \text{blkdiag}((\mathbf{0}, (\hat{\mathbf{h}}_k \hat{\mathbf{h}}_k^H + \boldsymbol{\Sigma}_k), \dots, (\hat{\mathbf{h}}_k \hat{\mathbf{h}}_k^H + \boldsymbol{\Sigma}_k)) + \frac{\sigma^2}{P} \mathbf{I}_{N(K+M+1)}, \quad (42)$$

$$\mathbf{V}_k = \mathbf{U}_k - \text{blkdiag}(\mathbf{0}, \dots, \underbrace{\hat{\mathbf{h}}_k \hat{\mathbf{h}}_k^H}_{(k+1)\text{-th block}}, \dots, \mathbf{0}). \quad (43)$$

However, we observe that the minimum function in (35) is non-smooth, which makes the given problem of the SE maximization problem for RSMA hard to solve. To resolve this, we use the LogSumExp technique in [24], [25] to approximate the minimum function involved in (35). This gives

$$\min_{j=1, \dots, Q} \{x_j\} \approx -\frac{1}{\eta} \log \left(\frac{1}{Q} \sum_{j=1}^Q \exp(-\eta x_j) \right), \quad (44)$$

$$\triangleq f(\{x_j\}_{j \in [Q]}), \quad (45)$$

where the larger η leads to the tighter approximation. Next, we rewrite the beam gain $G(\mathbf{P}; \theta)$ in (31) to express it as a more succinct form using the vector $\bar{\mathbf{p}}$ as follows:

$$G(\mathbf{P}; \theta) = P \cdot \mathbf{a}^H(\theta) \mathbf{P} \mathbf{P}^H \mathbf{a}(\theta) \quad (46)$$

$$= P \cdot \left((\mathbf{a}^T(\theta) \mathbf{P}^*) \otimes \mathbf{a}^H(\theta) \right) \text{vec}(\mathbf{P}) \quad (47)$$

$$= P \cdot \left(\left((\mathbf{I} \otimes \mathbf{a}^T(\theta)) \text{vec}(\mathbf{P}^*) \right)^T \otimes \mathbf{a}^H(\theta) \right) \text{vec}(\mathbf{P}) \quad (48)$$

$$= \bar{\mathbf{p}}^H \left(P \cdot \mathbf{I} \otimes \mathbf{a}(\theta) \otimes \mathbf{a}^H(\theta) \right) \bar{\mathbf{p}} \quad (49)$$

$$\triangleq \bar{\mathbf{p}}^H \mathbf{A}(\theta) \bar{\mathbf{p}}, \quad (50)$$

where (47), (48) come from $\text{vec}(\mathbf{XYZ}) = (\mathbf{Z}^T \otimes \mathbf{X}) \text{vec}(\mathbf{Y})$. With (50), the beam pattern MSE expression in (31) is rewritten by

$$\text{MSE}_r = \frac{1}{L} \sum_{u=1}^L |\bar{\mathbf{p}}^H \mathbf{A}(\theta_u) \bar{\mathbf{p}} - \bar{\mathbf{p}}^H \mathbf{T}(\theta_u) \bar{\mathbf{p}}|^2, \quad (51)$$

where $\mathbf{T}(\theta_u) = P \cdot t(\theta_u) \cdot \mathbf{I}_{N(K+M+1)}$.

As a result, \mathcal{P}_1 is reformulated as \mathcal{P}_2 :

$$\mathcal{P}_2 : \underset{\bar{\mathbf{p}}}{\text{maximize}} \quad \bar{R}_c^{\text{LSE}}(\bar{\mathbf{p}}) + \sum_{k=1}^K \bar{R}_k(\bar{\mathbf{p}}) \quad (52)$$

$$\text{subject to } \frac{1}{L} \sum_{u=1}^L |\bar{\mathbf{p}}^H \mathbf{A}(\theta_u) \bar{\mathbf{p}} - \bar{\mathbf{p}}^H \mathbf{T}(\theta_u) \bar{\mathbf{p}}|^2 \leq T_{\text{mse}}, \quad (53)$$

where $\bar{R}_c^{\text{LSE}}(\bar{\mathbf{p}})$, $\bar{R}_k(\bar{\mathbf{p}})$ are given by

$$\bar{R}_c^{\text{LSE}}(\bar{\mathbf{p}}) = f \left(\left\{ \frac{\bar{\mathbf{p}}^H \mathbf{U}_c(k) \bar{\mathbf{p}}}{\bar{\mathbf{p}}^H \mathbf{V}_c(k) \bar{\mathbf{p}}} \right\}_{k \in [K]} \right), \quad (54)$$

$$\bar{R}_k(\bar{\mathbf{p}}) = \log_2 \frac{\bar{\mathbf{p}}^H \mathbf{U}_k \bar{\mathbf{p}}}{\bar{\mathbf{p}}^H \mathbf{V}_k \bar{\mathbf{p}}}. \quad (55)$$

Note that the power constraint $\|\mathbf{P}\|_{\text{F}}^2 = 1$ in \mathcal{P}_1 is also removed in \mathcal{P}_2 , as this constraint will be incorporated into our proposed algorithm. Notwithstanding this reformulation, directly tackling \mathcal{P}_2 is still infeasible because evaluating SINR expressions with (40)-(43) requires the error covariance matrix Σ_k , which has not been determined. In the next section, we explain challenges in obtaining Σ_k and provide our approach to approximate Σ_k .

IV. ERROR COVARIANCE MATRIX ESTIMATION

Incorporating the error covariance matrix Σ_k in \mathcal{P}_2 is important to reflect knowledge of CSIT imperfections into the precoder design. In conventional approaches, we can obtain Σ_k through (i) Bayesian estimation or (ii) Frequentist approach. In Bayesian estimation, we assume that the channel statistics are known in the BS. For example, by modeling the DL channel as a Gaussian distribution with a known covariance, a closed-form expression for the error covariance can be derived, provided that certain CSI feedback is available [8], [25]. In the Frequentist approach, we use DL channel error samples to empirically calculate Σ_k as shown in [32].

In the case considered in this paper, we can easily find that neither approach is feasible. This limitation arises mainly because the BS cannot obtain CSI error statistics or error samples without feedback [24], whereas we do not rely on any direct CSI feedback. To address this, we exploit the CRLB to approximate the CSI error level produced by the UL training process. This approach is validated by the observation that 2D-NOMP can achieve near-optimal MSE [22], [23], which implies proximity to the CRLB. However, obtaining the CRLB typically requires ground-truth channel parameters [33], which cannot be obtained in our setup. To avoid this problem, we rely on the *observed Fisher information* [34]. Specifically, observed Fisher information is the instantaneous amount of information calculated after observing a specific sample, while Fisher information measures the expected amount of information. To this end, we define the UL channel parameter set \mathcal{P}_k as

$$\mathcal{P}_k = \{p_{k,1}, \dots, p_{k,L_k}\} \in \mathbb{C}^{4L_k \times 1}, \quad (56)$$

$$p_{k,\ell} = \left\{ \Re\{\alpha_{k,\ell}^{\text{ul}}\}, \Im\{\alpha_{k,\ell}^{\text{ul}}\}, \tau_{k,\ell}^{\text{ul}}, \theta_{k,\ell}^{\text{ul}} \right\} \in \mathbb{C}^{4 \times 1}. \quad (57)$$

Based on this, we find the observed Fisher information by computing the negative Hessian of the log-likelihood composed with an instantaneously estimated parameter $\hat{\mathcal{P}}_k$:

$$\mathbf{I}(\hat{\mathcal{P}}_k) = - \left. \frac{\partial^2 \log \mathcal{L}(\mathcal{P}_k; \mathbf{y}_k)}{\partial \mathcal{P}_k \partial \mathcal{P}_k^{\text{T}}} \right|_{\mathcal{P}_k = \hat{\mathcal{P}}_k} \in \mathbb{C}^{4L_k \times 4L_k}, \quad (58)$$

and the each element of (58) is given by (See [24]),

$$[\mathbf{I}(\hat{\mathcal{P}}_k)]_{u,v} = \frac{2}{\sigma^2} \Re \left(\sum_{n,s} \frac{\partial \bar{\mathbf{y}}_{k,n,s}^*}{\partial \mathcal{P}_u} \frac{\partial \bar{\mathbf{y}}_{k,n,s}}{\partial \mathcal{P}_v} - (\mathbf{y}_{k,n,s}^* - \bar{\mathbf{y}}_{k,n,s}^*) \frac{\partial^2 \bar{\mathbf{y}}_{k,n,s}}{\partial \mathcal{P}_u \partial \mathcal{P}_v} \right) \Bigg|_{\mathcal{P}_k = \hat{\mathcal{P}}_k}, \quad (59)$$

where $\mathbf{y}_{k,n,s}$ denotes the UL received signal at the n -th antenna and s -th resource block for user k (in (7)) and $\bar{\mathbf{y}}_{k,n,s}$ is the UL reconstructed signal defined with the parameter set \mathcal{P}_k , i.e.,

$$\bar{\mathbf{y}}_{k,n,s} \triangleq \sum_{\ell=1}^{L_k} \alpha_{k,\ell}^{\text{ul}} [\mathbf{u}(\tau_{k,\ell}^{\text{ul}}, \theta_{k,\ell}^{\text{ul}})]_{n,s}, \quad (60)$$

where $[\mathbf{u}(\tau_{k,\ell}^{\text{ul}}, \theta_{k,\ell}^{\text{ul}})]_{n,s}$ is given in (6).

Interestingly, [35] demonstrated that the inverse of the observed Fisher information provides the optimal performance in estimating the squared error realized. To apply this to the DL case, we utilize the Jacobian transformation as follows:

$$\mathbf{Q}_k^{\text{H}}(f) \mathbf{I}^{-1}(\hat{\mathcal{P}}_k) \mathbf{Q}_k(f) = \arg \min_{\hat{\Sigma}_k} \mathbb{E} \left[\sum_{m=1}^N \left[\mathbf{e}_k \mathbf{e}_k^{\text{H}} - \hat{\Sigma}_k \right]_{m,m}^2 \right], \quad (61)$$

where $\mathbf{Q}_k^{\text{H}}(f)$ denotes the Jacobian matrix at the frequency difference f and its derivation is straightforward, thus we omit here (refer to [22]). To relate this with our case, we can find that the observed Fisher information can be used to minimize the upper bound of error covariance matrix estimation for diagonal elements, i.e.,

$$\sum_{m=1}^N \left[\mathbb{E} \left[\mathbf{e}_k \mathbf{e}_k^{\text{H}} \right] - \hat{\Sigma}_k \right]_{m,m}^2 \leq \mathbb{E} \left[\sum_{m=1}^N \left[\mathbf{e}_k \mathbf{e}_k^{\text{H}} - \hat{\Sigma}_k \right]_{m,m}^2 \right]. \quad (62)$$

Using this, we estimate the error covariance matrix only with the diagonal component of (61). In [24], it was shown that the MSE predicted by our method (the trace of (61)) closely matches the actual MSE. This implies that at least the diagonal components of the error covariance matrix can be accurately estimated with (61), allowing Σ_k to be approximated as follows.

$$\Sigma_k \approx \left(\mathbf{Q}_k^{\text{H}}(f) \mathbf{I}^{-1}(\hat{\mathcal{P}}_k) \mathbf{Q}_k(f) \right) \circ \mathbf{I}_N \quad (63)$$

$$= \begin{bmatrix} \sigma_{k,1} & 0 & \cdots & 0 \\ 0 & \sigma_{k,2} & \cdots & 0 \\ \vdots & \vdots & \ddots & \vdots \\ 0 & 0 & \cdots & \sigma_{k,N} \end{bmatrix} = \hat{\Sigma}_k, \quad (64)$$

where $\sigma_{k,n}$ denotes the MSE at antenna n for user k . We note that the diagonal error covariance matrix is the case in which uncorrelated channel estimation errors are encountered for each antenna, which is widely assumed for the rich scattering channel where the spatial correlation of the channel is limited [32]. By replacing Σ_k in (40)-(43) with $\hat{\Sigma}_k$, we are ready to solve problem \mathcal{P}_2 .

V. PRECODER OPTIMIZATION

In this section, we propose a precoder optimization technique that addresses the problem of maximization of the SE sum under the MSE constraint for the detection of the beam pattern, which guarantees the desired design of the beam pattern. To address this, we first observe that the optimal solutions to problem \mathcal{P}_2 adhere to the KKT conditions, which serve as the foundation for our proposed technique. The KKT conditions are summarized as follows:

- (i) **Primal feasibility:** To be a feasible solution of given problem, the precoder must satisfy the given constraint, i.e., the inequality constraint in (53).
- (ii) **Dual feasibility:** For the dual problem, the Lagrange multiplier should be greater than or equal to 0, i.e., $\nu \geq 0$.
- (iii) **Complementary slackness:** It refers to a relationship between the inequality constraints and their corresponding Lagrange multipliers, which represents

$$\nu \left(\frac{1}{L} \sum_{\ell=1}^L |\bar{\mathbf{p}}^H \mathbf{A}(\theta_\ell) \bar{\mathbf{p}} - \bar{\mathbf{p}}^H \mathbf{T}(\theta_\ell) \bar{\mathbf{p}}|^2 - T_{\text{mse}} \right) = 0. \quad (65)$$

- (iv) **Stationarity condition:** The condition denotes the gradient of the Lagrangian with respect to the optimization variable $\bar{\mathbf{p}}$ is equal to zero.

Upon this, we summarize the stationarity condition for the dual problem of \mathcal{P}_2 with the following lemma.

Lemma 1. *The stationarity condition for the dual problem of \mathcal{P}_2 holds if the following equation is satisfied:*

$$\mathbf{L}(\bar{\mathbf{p}}, \nu) \bar{\mathbf{p}} = \zeta(\bar{\mathbf{p}}, \nu) \mathbf{R}(\bar{\mathbf{p}}, \nu) \bar{\mathbf{p}}, \quad (66)$$

where

$$\begin{aligned} \mathbf{L}(\bar{\mathbf{p}}, \nu) &= \zeta_{\text{num}}(\bar{\mathbf{p}}, \nu) \times \\ &\left[\sum_{k=1}^K \left\{ \frac{\exp\left(-\eta \frac{\bar{\mathbf{p}}^H \mathbf{U}_c(k) \bar{\mathbf{p}}}{\bar{\mathbf{p}}^H \mathbf{V}_c(k) \bar{\mathbf{p}}}\right)}{\sum_{j=1}^K \exp\left(-\eta \log_2 \frac{\bar{\mathbf{p}}^H \mathbf{U}_c(j) \bar{\mathbf{p}}}{\bar{\mathbf{p}}^H \mathbf{V}_c(j) \bar{\mathbf{p}}}\right)} \right\} \frac{\mathbf{V}_c(k)}{\bar{\mathbf{p}}^H \mathbf{V}_c(k) \bar{\mathbf{p}}} + \sum_{k=1}^K \left(\frac{\mathbf{V}_k}{\bar{\mathbf{p}}^H \mathbf{V}_k \bar{\mathbf{p}}} \right) \right. \\ &\left. + \frac{4\nu \log 2}{LP^2} \sum_{u=1}^L \left((\bar{\mathbf{p}}^H \mathbf{A}(\theta_u) \bar{\mathbf{p}}) \mathbf{A}(\theta_u) + (\bar{\mathbf{p}}^H \mathbf{T}(\theta_u) \bar{\mathbf{p}}) \mathbf{T}(\theta_u) \right) \bar{\mathbf{p}} \right], \end{aligned} \quad (67)$$

$$\begin{aligned} \mathbf{R}(\bar{\mathbf{p}}, \nu) &= \zeta_{\text{den}}(\bar{\mathbf{p}}, \nu) \times \\ &\left[\sum_{k=1}^K \left\{ \frac{\exp\left(-\eta \frac{\bar{\mathbf{p}}^H \mathbf{U}_c(k) \bar{\mathbf{p}}}{\bar{\mathbf{p}}^H \mathbf{V}_c(k) \bar{\mathbf{p}}}\right)}{\sum_{j=1}^K \exp\left(-\eta \log_2 \frac{\bar{\mathbf{p}}^H \mathbf{U}_c(j) \bar{\mathbf{p}}}{\bar{\mathbf{p}}^H \mathbf{V}_c(j) \bar{\mathbf{p}}}\right)} \right\} \frac{\mathbf{U}_c(k)}{\bar{\mathbf{p}}^H \mathbf{U}_c(k) \bar{\mathbf{p}}} + \sum_{k=1}^K \left(\frac{\mathbf{U}_k}{\bar{\mathbf{p}}^H \mathbf{U}_k \bar{\mathbf{p}}} \right) \right. \\ &\left. + \frac{4\nu \log 2}{LP^2} \sum_{u=1}^L \left((\bar{\mathbf{p}}^H \mathbf{A}(\theta_u) \bar{\mathbf{p}}) \mathbf{T}(\theta_u) + (\bar{\mathbf{p}}^H \mathbf{T}(\theta_u) \bar{\mathbf{p}}) \mathbf{A}(\theta_u) \right) \right], \end{aligned} \quad (68)$$

in which ν in (67) and (68) denotes the Lagrangian multiplier, and we define $\zeta(\bar{\mathbf{p}}, \nu)$ as

$$\begin{aligned} \zeta(\bar{\mathbf{p}}, \nu) &= \left\{ \frac{1}{K} \sum_{k=1}^K \exp\left(-\eta \log_2 \left(\frac{\bar{\mathbf{p}}^H \mathbf{U}_c(k) \bar{\mathbf{p}}}{\bar{\mathbf{p}}^H \mathbf{V}_c(k) \bar{\mathbf{p}}} \right) \right) \right\}^{-\frac{1}{\eta \log_2 e}} \\ &\times \prod_{k=1}^K \frac{\bar{\mathbf{p}}^H \mathbf{U}_k \bar{\mathbf{p}}}{\bar{\mathbf{p}}^H \mathbf{V}_k \bar{\mathbf{p}}} \times 2^{\nu \left(\frac{1}{LP^2} \sum_{u=1}^L |\bar{\mathbf{p}}^H \mathbf{A}(\theta_u) \bar{\mathbf{p}} - \bar{\mathbf{p}}^H \mathbf{T}(\theta_u) \bar{\mathbf{p}}|^2 - \frac{T_{\text{mse}}}{P^2} \right)} \end{aligned} \quad (69)$$

$$= \frac{\zeta_{\text{num}}(\bar{\mathbf{p}}, \nu)}{\zeta_{\text{den}}(\bar{\mathbf{p}}, \nu)}. \quad (70)$$

However, note that even if we can find a precoding vector that satisfies the KKT conditions in (i)-(iv), it still does not imply that it is the global optimal point, since the underlying problem of (52) remains non-convex. Instead, only a necessary condition of the local optimal point is ensured by jointly finding the precoding vector $\bar{\mathbf{p}}$ and the Lagrangian multiplier

Algorithm 1: GPI-ISAC-RS Algorithm

Input: UL received signal, $\mathbf{y}_k \in \mathbb{C}^{MN \times 1}$
Output: DL precoder, $\bar{\mathbf{p}}^* \in \mathbb{C}^{N(K+M+1) \times 1}$
Initialize: $\bar{\mathbf{p}}^{(0)}, \nu^{(0)}$;
Set each iteration count as $t = 1, n = 1$;
Reconstruct the DL channel $\hat{\mathbf{h}}_k, \forall k$ via Section III;
Estimate the error covariance $\hat{\Sigma}_k, \forall k$ via Section IV;
while $|\nu^{(n)} - \nu^{(n-1)}| \geq \epsilon_\nu$ **or** $n \leq n_{\text{max}}$ **do**
 Set the iteration count $t = 1$;
 while $\|\bar{\mathbf{p}}^{(t)} - \bar{\mathbf{p}}^{(t-1)}\| \geq \epsilon_p$ **or** $t \leq t_{\text{max}}$ **do**
 Construct matrix $\mathbf{L}(\bar{\mathbf{p}}^{(t-1)}, \nu^{(n)})$ with (33);
 Construct matrix $\mathbf{R}(\bar{\mathbf{p}}^{(t-1)}, \nu^{(n)})$ with (34);
 Compute matrix $\mathbf{K}(\bar{\mathbf{p}}^{(t-1)}, \nu^{(n)}) \leftarrow$
 $\mathbf{R}^{-1}(\bar{\mathbf{p}}^{(t-1)}, \nu^{(n)}) \mathbf{L}(\bar{\mathbf{p}}^{(t-1)}, \nu^{(n)})$;
 Update $\bar{\mathbf{p}}(t)$ as:

$$\bar{\mathbf{p}}^{(t)} \leftarrow \frac{\mathbf{K}(\bar{\mathbf{p}}^{(t-1)}, \nu^{(n)}) \bar{\mathbf{p}}^{(t-1)}}{\|\mathbf{K}(\bar{\mathbf{p}}^{(t-1)}, \nu^{(n)}) \bar{\mathbf{p}}^{(t-1)}\|},$$

 $t \leftarrow t + 1$;
 end
 if $\zeta_{\text{mse}} > \frac{1}{L} \sum_{\ell=1}^L |G(\mathbf{P}; \theta_\ell) - P \cdot t(\theta_\ell)|^2$ **then**
 $\nu^{(n+1)} \leftarrow \frac{\nu^{(n)} + \nu_{\text{min}}}{2}$;
 else
 $\nu^{(n+1)} \leftarrow \frac{\nu^{(n)} + \nu_{\text{max}}}{2}$;
 end
 $n \leftarrow n + 1$;
end
 $\bar{\mathbf{p}}^* \leftarrow \bar{\mathbf{p}}(t-1)$;
return $\bar{\mathbf{p}}^*$;

ν that satisfies the KKT conditions. Furthermore, it should be noted that the Lagrange multiplier ν affects the optimal precoder $\bar{\mathbf{p}}^*$, and vice versa, thus the interdependence makes it challenging to optimize $\bar{\mathbf{p}}$ and ν simultaneously.

To address this problem, we first highlight the relationship between the objective function in (52) and $\zeta(\bar{\mathbf{p}}, \nu)$ in (66), under the assumption that the KKT conditions hold. Specifically, if a precoder and Lagrange multiplier pair $(\bar{\mathbf{p}}^*, \nu^*)$ satisfies the complementary slackness, then the following holds:

$$\log_2 \zeta(\bar{\mathbf{p}}^*, \nu^*) = \bar{R}_c^{\text{LSE}}(\bar{\mathbf{p}}^*) + \sum_{k=1}^K \bar{R}_k(\bar{\mathbf{p}}^*), \quad (71)$$

where the MSE constraint term in (69) vanishes, and $\zeta(\bar{\mathbf{p}}^*, \nu^*)$ is simply the sum SE, i.e., our objective function. Therefore, insofar as the KKT conditions are satisfied, we just need to find $(\bar{\mathbf{p}}^*, \nu^*)$ that maximizes $\zeta(\bar{\mathbf{p}}^*, \nu^*)$, which is equivalent to maximizing the objective of \mathcal{P}_2 .

Based on this, we revisit the stationarity condition in Lemma 1 and interpret the problem of maximizing $\zeta(\bar{\mathbf{p}}, \nu)$ as a form of NEPv [2], [25]. We focus on $\zeta(\bar{\mathbf{p}}, \nu)$ by multiplying the inverse of $\mathbf{R}(\bar{\mathbf{p}}, \nu)$ on both sides of (66), which is given by

$$\mathbf{R}^{-1}(\bar{\mathbf{p}}, \nu) \mathbf{L}(\bar{\mathbf{p}}, \nu) \bar{\mathbf{p}} = \zeta(\bar{\mathbf{p}}, \nu) \bar{\mathbf{p}}. \quad (72)$$

With this, assuming only the update of $\bar{\mathbf{p}}$ while keeping ν fixed, we summarize our precoder design objective as follows:

Proposition 1. Suppose a Lagrange multiplier $\nu^\dagger \geq 0$ is given, and define the optimal precoder \mathbf{p}^\dagger as the vector that maximizes the objective function $\zeta(\bar{\mathbf{p}}, \nu^\dagger)$ for the fixed ν^\dagger , under the stationarity condition in (72), which satisfies

$$\mathbf{R}^{-1}(\bar{\mathbf{p}}, \nu^\dagger) \mathbf{L}(\bar{\mathbf{p}}, \nu^\dagger) \bar{\mathbf{p}} = \zeta(\bar{\mathbf{p}}, \nu^\dagger) \bar{\mathbf{p}}.$$

Then, \mathbf{p}^\dagger is the leading eigenvector of the matrix $\mathbf{K}(\bar{\mathbf{p}}, \nu^\dagger) \triangleq \mathbf{R}^{-1}(\bar{\mathbf{p}}, \nu^\dagger) \mathbf{L}(\bar{\mathbf{p}}, \nu^\dagger)$.

This proposition provides an useful insight, as it allows the problem of maximizing $\zeta(\bar{\mathbf{p}}, \nu^\dagger)$ to be interpreted as a form of NEPv. Specifically, $\zeta(\bar{\mathbf{p}}, \nu^\dagger)$ is cast as a nonlinear eigenvalue of the matrix $\mathbf{K}(\bar{\mathbf{p}}, \nu^\dagger)$ and $\bar{\mathbf{p}}$ is the corresponding eigenvector.

Inspired by [2], [25], we can find the leading eigenvector of $\mathbf{K}(\bar{\mathbf{p}}, \nu^\dagger)$ with the generalized power iteration (GPI) method. In particular, we repeatedly update the precoder to be projected into the maxtrix $\mathbf{K}(\bar{\mathbf{p}}, \nu^\dagger)$ and be normalized to ensure the original power constraint in (34). Specifically, at t -th iteration, we update the precoder as

$$\bar{\mathbf{p}}^{(t)} \leftarrow \frac{\mathbf{K}(\bar{\mathbf{p}}^{(t-1)}, \nu^\dagger) \bar{\mathbf{p}}^{(t-1)}}{\|\mathbf{K}(\bar{\mathbf{p}}^{(t-1)}, \nu^\dagger) \bar{\mathbf{p}}^{(t-1)}\|}, \quad (73)$$

and this process is repeated until the termination criterion is met. For example, we expect that it is converged when $|\bar{\mathbf{p}}^{(t)} - \bar{\mathbf{p}}^{(t-1)}| < \epsilon$, where ϵ is small enough.

To understand how the proposed method maximizes the nonlinear eigenvalue $\zeta(\bar{\mathbf{p}}, \nu^\dagger)$, we represent the inner product of denominator in (73) with an arbitrary precoder $\bar{\mathbf{p}}$ as follows:

$$\begin{aligned} (\mathbf{K}(\bar{\mathbf{p}}^{(t-1)}, \nu^\dagger) \bar{\mathbf{p}}^{(t-1)})^H \bar{\mathbf{p}} &= (\mathbf{K}(\bar{\mathbf{p}}^{(t-1)}, \nu^\dagger) \bar{\mathbf{p}}^\dagger)^H \bar{\mathbf{p}} \\ &+ (\bar{\mathbf{p}}^{(t-1)} - \bar{\mathbf{p}}^\dagger)^H \nabla_{\bar{\mathbf{p}}^{(t-1)}} (\mathbf{K}(\bar{\mathbf{p}}^\dagger, \nu^\dagger) \bar{\mathbf{p}}^\dagger) \bar{\mathbf{p}} + o(\|\bar{\mathbf{p}}^{(t-1)} - \bar{\mathbf{p}}^\dagger\|), \end{aligned} \quad (74)$$

Assuming that there exists a set of basis $\{\bar{\mathbf{p}}^\dagger, \mathbf{v}_2, \dots, \mathbf{v}_{N(K+M+1)}\}$ for the matrix $\mathbf{K}(\bar{\mathbf{p}}^{(t-1)}, \nu^\dagger)$, we also rewrite (74) as

$$\begin{aligned} (\mathbf{K}(\bar{\mathbf{p}}^{(t-1)}, \nu^\dagger) \bar{\mathbf{p}}^{(t-1)})^H \bar{\mathbf{p}} &= \alpha_1 (\mathbf{K}(\bar{\mathbf{p}}^{(t-1)}, \nu^\dagger) \bar{\mathbf{p}}^{(t-1)})^H \bar{\mathbf{p}}^\dagger \\ &+ \sum_{i=2}^{N(K+M+1)} \alpha_i (\mathbf{K}(\bar{\mathbf{p}}^{(t-1)}, \nu^\dagger) \bar{\mathbf{p}}^{(t-1)})^H \mathbf{v}_i, \end{aligned} \quad (75)$$

since $\bar{\mathbf{p}}$ can be expressed as $\alpha_1 \bar{\mathbf{p}}^\dagger + \sum_{i=2}^{N(K+M+1)} \alpha_i \mathbf{v}_i$ by using a basis set.

Now, considering that $\mathbf{K}(\bar{\mathbf{p}}^\dagger, \nu^\dagger) \bar{\mathbf{p}}^\dagger = \lambda^\dagger \bar{\mathbf{p}}^\dagger$ holds, we obtain from (74)

$$[(\mathbf{K}(\bar{\mathbf{p}}^{(t-1)}, \nu^\dagger) \bar{\mathbf{p}}^{(t-1)})^H \bar{\mathbf{p}}^\dagger]^2 = [\lambda^\dagger + o(\|\bar{\mathbf{p}}^{(t-1)} - \bar{\mathbf{p}}^\dagger\|)]^2. \quad (76)$$

We also derive an upper bound for the sum of the inner product of the remaining orthonormal basis, $\{\mathbf{v}_i\}_{i=2, \dots, N(K+M+1)}$, as follows.

$$\sum_{i=2}^{N(K+M+1)} [(\mathbf{K}(\bar{\mathbf{p}}^{(t-1)}, \nu^\dagger) \bar{\mathbf{p}}^{(t-1)})^H \mathbf{v}_i]^2 \quad (77)$$

$$\leq \sum_{i=2}^{N(K+M+1)} [\lambda_i^2 ((\bar{\mathbf{p}}^{(t-1)})^H \mathbf{v}_i)^2 + 2\lambda_i ((\bar{\mathbf{p}}^{(t-1)})^H \mathbf{v}_i) + o(\|\bar{\mathbf{p}}^{(t-1)} - \bar{\mathbf{p}}^\dagger\|)^2] \quad (78)$$

$$\leq [\lambda_2 \|\bar{\mathbf{p}}^{(t-1)} - \bar{\mathbf{p}}^\dagger\| + o(\|\bar{\mathbf{p}}^{(t-1)} - \bar{\mathbf{p}}^\dagger\|)]^2, \quad (79)$$

which is based on the following fact:

$$\begin{aligned} \sum_{i=2}^{N(K+M+1)} ((\bar{\mathbf{p}}^{(t-1)})^H \mathbf{v}_i)^2 &= 1 - ((\bar{\mathbf{p}}^{(t-1)})^H \bar{\mathbf{p}}^\dagger)^2 \quad (80) \\ &\leq 2(1 - (\bar{\mathbf{p}}^{(t-1)})^H \bar{\mathbf{p}}^\dagger) \leq \|\bar{\mathbf{p}}^{(t-1)} - \bar{\mathbf{p}}^\dagger\|^2. \quad (81) \end{aligned}$$

By comparing (76) with (79), given that $\bar{\mathbf{p}}^{(t-1)}$ is close enough to $\bar{\mathbf{p}}^\dagger$, iteratively projecting the precoder $\bar{\mathbf{p}}^{(t-1)}$ onto $\mathbf{K}(\bar{\mathbf{p}}^{(t-1)}, \nu^\dagger)$ makes the non-leading eigenvectors $\{\mathbf{v}_i\}_{i=2, \dots, N(K+M+1)}$ vanish, while the leading eigenvector $\bar{\mathbf{p}}^\dagger$ remains, as $|\lambda^\dagger| > |\lambda_i|$, $\forall i \geq 2$. Therefore, our proposed algorithm approaches the leading eigenvector $\bar{\mathbf{p}}^\dagger$.

Recall that, so far, we have assumed the given Lagrange multiplier $\nu = \nu^\dagger$, and our rationale holds as long as the KKT condition is satisfied. Now, to ensure this, we explore how to update ν accordingly. First, ν must be non-negative due to dual feasibility, and it must also satisfy complementary slackness when multiplied by the inequality constraints in the dual problem. Meanwhile, the gradient component related to the MSE constraint in (67), (68) is linearly proportional to ν , which implies that the design objectives can be adjusted based on the value of ν . We summarize this in the following remark.

Remark 1. (Trade-off between communication and sensing) Notably, Lagrange multiplier ν dictates the design direction between communication and sensing. If we find a precoder $\bar{\mathbf{p}}$ that maximizes $\zeta(\bar{\mathbf{p}}, \nu)$ with ν close to zero, it indicates that the given MSE constraint is loose, allowing us to focus on optimizing the precoder to maximize the sum SE without considering the sensing constraint. In contrast, when we increase the value of ν , we obtain the precoder solution with more highlights in the MSE constraint for the dual problem, which is indeed not favorable to communication performance due to the trade-off relationship between sensing and communication.

Following the intuition of the above remark, we choose ν to be as small as possible, provided that it satisfies the MSE constraints of the detection beam pattern. In this regard, we employ a binary tree search method. Specifically, we begin with a ν value of zero and derive the optimal precoder that maximizes the sum SE using the NEPv interpretation. We then verify whether this solution meets the MSE constraint. If the feasibility conditions are not satisfied, we increase the ν value to more account for the MSE constraint in the next iteration. In contrast, if the solution meets the constraints, we attempt to decrease the ν value to achieve smaller feasible values. Through this approach, we effectively find the smallest ν that satisfies all KKT conditions, which we denote ν^* . With this, we repeat the process in (73) and obtain the corresponding precoding vector $\bar{\mathbf{p}}^*$. In conclusion, we alternatively optimize $(\bar{\mathbf{p}}, \nu)$ with our proposed method, which is summarized in **Algorithm 1**.

VI. SIMULATION RESULTS

In this section, we demonstrate the performance of the proposed method in various settings. First, for comparison, we present existing state-of-the-art ISAC precoding methods as follows:

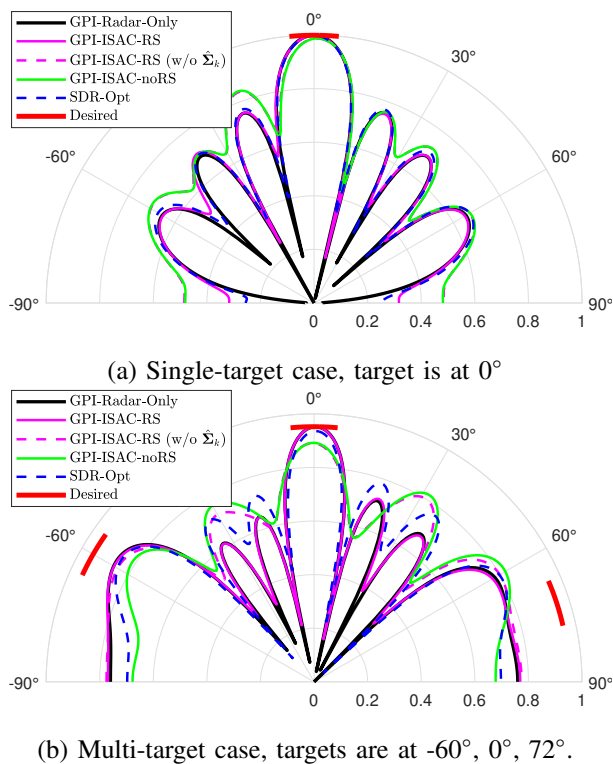


Fig. 2: Beam pattern example for $N = 8, K = 4, M = 4$.

- **GPI-ISAC (no RS):** As a recently proposed ISAC framework under imperfect CSIT [2], it considers the problem in (35); yet with conventional SDMA.
- **Semi-definite relaxation (SDR)-based method:** As shown in [3], [11], this method is based on the SDR technique, which solves the following problem:

$$\underset{\mathbf{P}}{\text{minimize}} \text{MSE}_r \quad (82)$$

$$\text{subject to } \text{SINR}_k \geq \Gamma_k, \|\mathbf{P}\|_F^2 = 1, \quad (83)$$

thereafter we perform a rank-1 approximation to obtain feasible precoding vectors from the positive semi-definite matrix. In (82), it can be observed that the constraint and objective function are changed compared to the case of \mathcal{P}_1 in (35), indicating that the SDR-based method is a radar-centric approach as explained in [2]. In (83), we determine the SINR constraint Γ_k from GPI-ISAC for a fair comparison. If the algorithm fails to find a precoder set that satisfies the constraint, we reduce Γ_k for all k by 5% to make the problem feasible.

A. Sensing Beam Shaping for the Desired Target

In Fig. 2, we plot the beam patterns to investigate the sensing performance for each technique (with $\nu = \nu_{\max}$ for the GPI cases). This analysis includes both single-target and multi-target scenarios, with the desired targets specified in Fig. 2. First, the Radar-only technique introduced in [2] demonstrates the lowest sidelobe levels in both cases, resulting in the highest beam gain at the target angle. This is expected as these designs exclusively prioritize the sensing metric without considering

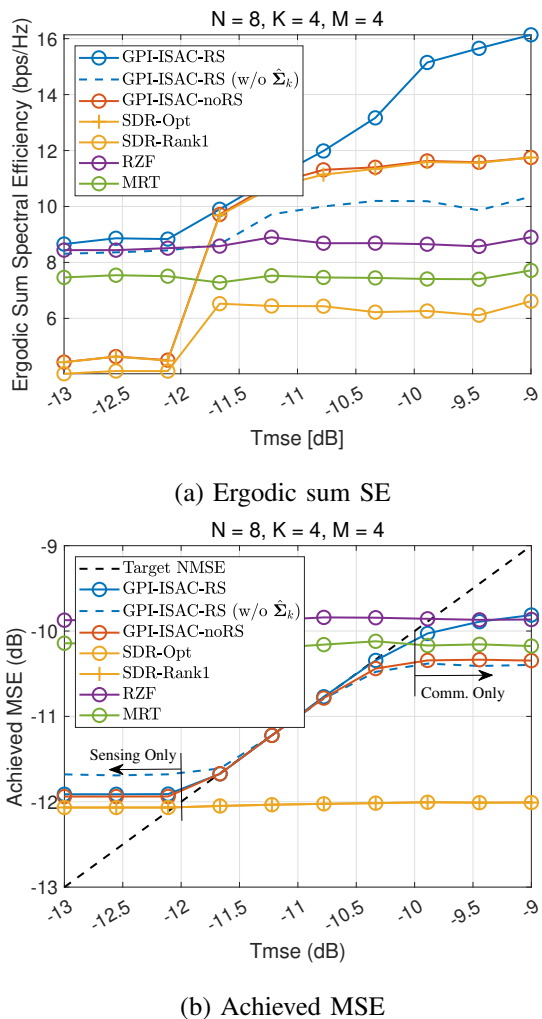


Fig. 3: (a) Achieved MSE and (b) Ergodic sum SE with $N = 8, K = 4, M = 4, \eta_{k,\ell} = 0.9 \forall (k, \ell)$, the SNR ($= P/\sigma^2$) of 35 dB is assumed.

the communication metric. In contrast, other ISAC-supported methods exhibit relatively higher sidelobe levels. Notably, our proposed method (GPI-ISAC-RS) achieves the lowest sidelobe levels while maintaining high beam gain for the target direction, suggesting that the method achieves the highest possible sensing performance compared to other approaches. Another notable observation is that when the error covariance matrix estimation is not applied in the proposed method, there is an increase in sidelobe levels and a degradation of beam gain at the target angle, leading to reduced sensing performance. This shows that, even though the error covariance matrix estimation is used mainly for the communication metric, it also impacts the sensing performance in ISAC systems where hardware resources are shared. Furthermore, the RS case exhibits improved maximum sensing performance compared to the RS case without RS. This can be attributed to the common message stream in the RS configuration, which, as seen in (51), contributes to improving the sensing performance for the sensing-centric regime.

B. Performance over Target MSE

1) *SE vs Target MSE*: In Fig. 3, we examine the ergodic sum SE and achieved MSE in (31) over the target MSE, T_{mse} . For a comprehensive comparison, we include communication-only methods such as MRT and RZF alongside ISAC-supported benchmarks. As shown in Fig. 3-(a), a lower MSE constraint results in a reduced SE for all ISAC methods, highlighting the trade-off relationship between sensing and communication. That is, focusing on beam pattern matching for a specific target with higher accuracy reduces communication performance, while prioritizing communication performance compromises sensing accuracy. Despite this, the proposed GPI-ISAC-RS achieves the best SE performance across all given target MSE levels. This relative performance gain becomes particularly pronounced at lower target MSE levels, which correspond to the sensing-oriented operational region. This indicates that the proposed RS-based method can maintain communication performance even when spatial resources are allocated to sensing targets [4]. In particular, we also observe that the proposed error covariance estimation method is crucial for achieving the RS gain. Without it, performance decreases significantly, even lower than that of the GPI-ISAC case in most of the target MSE region.

2) *Achieved MSE vs Target MSE*: The foundation of the SE gain becomes evident when analyzing the trends in the actual MSE achieved for each target MSE. In particular, when the radar beam pattern constraint is relaxed (higher T_{mse}), as shown in Fig. 3-(b), the actual MSE achieved by the proposed method adapts more effectively to the target MSE, contributing to SE gains. In other words, compared to the no-RS method, the additional common message stream in the proposed technique is used to maximize communication performance, resulting in a higher actual MSE but ultimately improves SE gains. On the other hand, when the constraint of the beam pattern is difficult to satisfy (lower T_{mse}), the proposed method does not show a significant improvement in the MSE performance compared to the case without RS. However, this radar-centric precoding approach can cause interference with communication functionality, which RS effectively manages to achieve SE gains. Crucially, it is observed that failing to estimate error covariance leads to suboptimal MSE performance. This highlights that accurately estimating the error covariance is of importance not only for communication performance but also for sensing performance.

C. Performance per SNR

In Fig. 4-(a), we represent the ergodic sum SE per SNR. Firstly, we recall that the SDR-based algorithm without rank-1 approximation achieves the same SE as GPI-ISAC (no RS) while providing a lower MSE. However, this approach is not practical, as feasible beamforming vectors require the rank-1 approximation. It also reveals that GPI-ISAC (no RS) provides higher SE than the SDR-based algorithm after rank-1 approximation (SDR-Rank1) and RZF for $T_{\text{mse}} = -11$ dB, while closely meeting the MSE constraint, as shown in Fig. 4-(b). In this regard, we observe that GPI-ISAC-noRS significantly outperforms SDR-Rank1 in terms of SE while

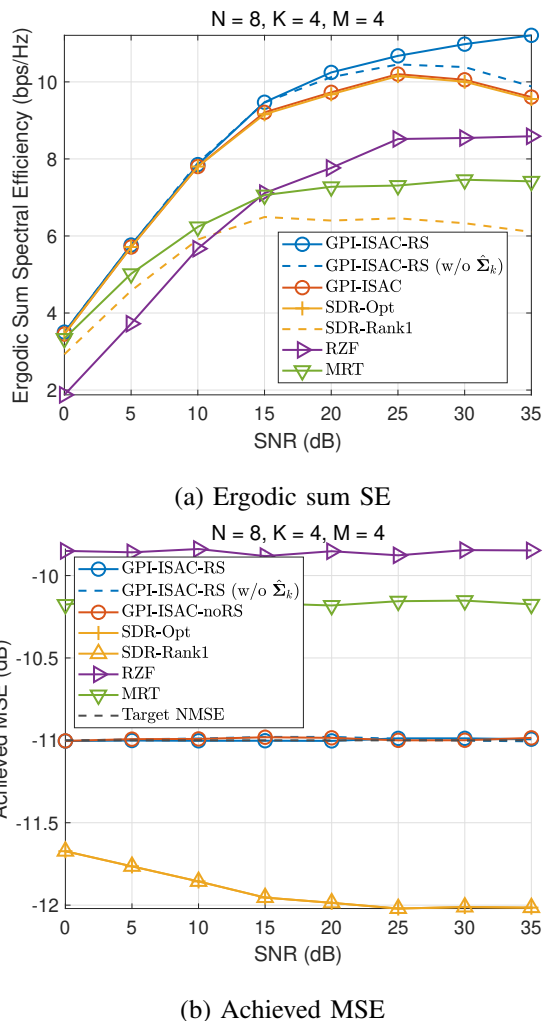
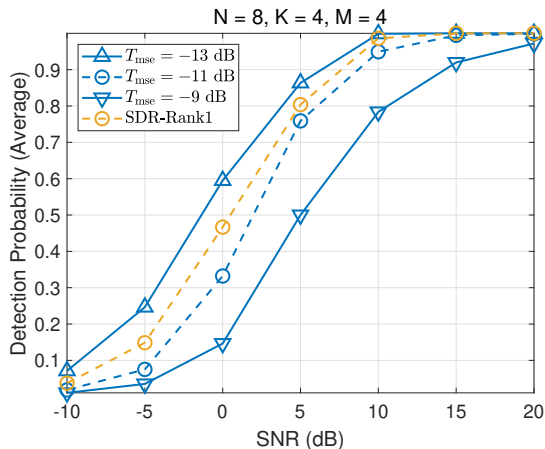
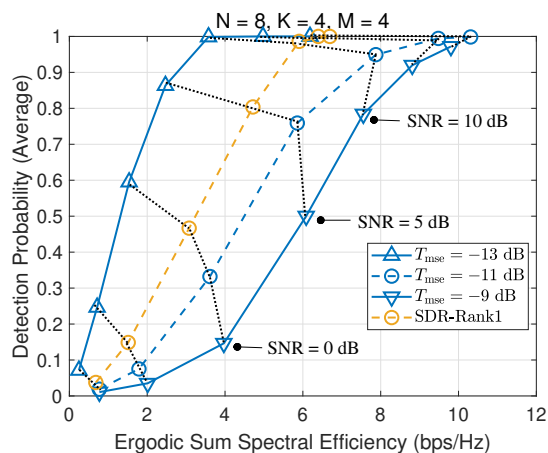


Fig. 4: (a) Ergodic sum SE and (b) Achieved MSE with $N = 8, K = 4, M = 4$ and $T_{\text{mse}} = -11$ dB.

satisfying the MSE constraints. This gap is mainly due to the fact that SDR-Rank1 is a radar-oriented ISAC beamforming algorithm as identified in Fig. 4-(b). Moreover, it is observed that the proposed RS-based ISAC precoding method achieves significant SE gains while maintaining the same MSE as the GPI-ISAC-noRS approach. This suggests that the proposed RS method effectively mitigates the increased multi-user interference caused by CSIT inaccuracies in zero-feedback scenarios.

D. Detection Probability

In Fig. 5-(a), we plot the detection probability as a function of the transmit SNR as studied in [36]. In particular, the range from -13 to 9 dB corresponds to the achievable region of our proposed method determined by adjustment of T_{mse} . When the MSE of the target is lower, a more accurate sensing beam is made, leading to a higher detection probability. Specifically, for $T_{\text{mse}} = -11$ dB, this region is considered suitable for ISAC, where sensing and communication are performed simultaneously. In this case, we compared the performance of the proposed method with the SDR-rank 1 approach. The SDR-based method, which solves (82)-(83) appears to improve the

(a) Average detection probability per SNR ($=P/\sigma^2$)

(b) Average detection probability vs. ergodic sum SE

Fig. 5: Average detection probability with $N = 8, K = 4, M = 4$, and $\eta_{k,\ell} = 0.9 \forall(k, \ell)$.

detection performance under the same T_{mse} . To investigate the trade-off in terms of SE, Fig. 5-(b) illustrates the ergodic sum SE corresponding to each point in Fig. 5-(a). Points connected by dashed lines represent the same transmit SNR. As expected, the SDR approach achieves better sensing performance, but falls short in SE compared to the proposed method. Interestingly, this trade-off relationship is evident up to an SNR of 0 dB. However, in higher SNR regions, the proposed method exhibits only marginally lower detection probability compared to the SDR-based approach, while offering substantial SE gains. This highlights the superiority of the proposed method in practical ISAC scenarios.

VII. CONCLUSION

This paper presents a precoding method for FDD MIMO ISAC systems that removes the need for channel feedback, thereby simultaneously supporting sensing and communication functionalities with low-latency characteristics. Specifically, we formulate a problem to maximize the sum SE under a beam pattern constraint based on MSE. By reconstructing the DL channel solely from UL training data, we mitigate

feedback overhead and address imperfections in CSIT through the estimation of the error covariance matrix. In addition, to mitigate interference between sensing and communication functionality, we consider RSMA that is known to provide robustness toward both objectives. Subsequently, we optimize the RSMA precoder using the KKT conditions to jointly update the precoding vector and Lagrange multipliers, wherein the principle of NEPv is used to resolve the non-convexity. Our extensive simulation results demonstrate that our method offers precise and versatile beam pattern control and substantial SE gains, outperforming current techniques in the sensing-communication performances.

APPENDIX A

PROOF OF LEMMA 1

We define the Lagrangian function as

$$\begin{aligned} \mathcal{L}(\bar{\mathbf{p}}, \nu) = & -\frac{1}{\eta} \log \left(\frac{1}{K} \sum_{k=1}^K \exp \left(-\eta \log_2 \left(\frac{\bar{\mathbf{p}}^H \mathbf{U}_c(k) \bar{\mathbf{p}}}{\bar{\mathbf{p}}^H \mathbf{V}_c(k) \bar{\mathbf{p}}} \right) \right) \right) \\ & + \sum_{k=1}^K \log_2 \left(\frac{\bar{\mathbf{p}}^H \mathbf{U}_k \bar{\mathbf{p}}}{\bar{\mathbf{p}}^H \mathbf{V}_k \bar{\mathbf{p}}} \right) \\ & + \nu \left(\frac{1}{LP^2} \sum_{\ell=1}^L \left| \bar{\mathbf{p}}^H \mathbf{A}(\theta_\ell) \bar{\mathbf{p}} - \bar{\mathbf{p}}^H \mathbf{T}(\theta_\ell) \bar{\mathbf{p}} \right|^2 - \frac{T_{\text{mse}}}{P^2} \right) \\ \triangleq & \log_2(\zeta(\bar{\mathbf{p}}, \nu)) \end{aligned} \quad (84)$$

By differentiating (85), we find that

$$\frac{\partial \mathcal{L}(\bar{\mathbf{p}}, \nu)}{\partial \bar{\mathbf{p}}} = \frac{\mathcal{L}(\bar{\mathbf{p}}, \nu)}{\partial \zeta(\bar{\mathbf{p}}, \nu)} \frac{\partial \zeta(\bar{\mathbf{p}}, \nu)}{\partial \bar{\mathbf{p}}} = \frac{1}{\zeta(\bar{\mathbf{p}}, \nu) \log 2} \frac{\partial \zeta(\bar{\mathbf{p}}, \nu)}{\partial \bar{\mathbf{p}}}. \quad (86)$$

For the stationarity condition, our aim is to find a precoder that satisfies $\partial \mathcal{L}(\bar{\mathbf{p}}, \nu) / \partial \bar{\mathbf{p}} = 0$, or equivalently (86) equal to zero. Accordingly, $\partial \zeta(\bar{\mathbf{p}}, \nu) / \partial \bar{\mathbf{p}}$ is given by

$$\begin{aligned} \frac{\partial \zeta(\bar{\mathbf{p}}, \nu)}{\partial \bar{\mathbf{p}}} = & \zeta(\bar{\mathbf{p}}, \nu) \left[\sum_{k=1}^K \left\{ \frac{\exp \left(-\eta \frac{\bar{\mathbf{p}}^H \mathbf{U}_c(k) \bar{\mathbf{p}}}{\bar{\mathbf{p}}^H \mathbf{V}_c(k) \bar{\mathbf{p}}} \right)}{\sum_{j=1}^K \exp \left(-\eta \log_2 \frac{\bar{\mathbf{p}}^H \mathbf{U}_c(j) \bar{\mathbf{p}}}{\bar{\mathbf{p}}^H \mathbf{V}_c(j) \bar{\mathbf{p}}} \right)} \right\} \right. \\ & \times \left(\frac{\mathbf{U}_c(k) \bar{\mathbf{p}}}{\bar{\mathbf{p}}^H \mathbf{U}_c(k) \bar{\mathbf{p}}} - \frac{\mathbf{V}_c(k) \bar{\mathbf{p}}}{\bar{\mathbf{p}}^H \mathbf{V}_c(k) \bar{\mathbf{p}}} \right) + \sum_{k=1}^K \left(\frac{\mathbf{U}_k \bar{\mathbf{p}}}{\bar{\mathbf{p}}^H \mathbf{U}_k \bar{\mathbf{p}}} - \frac{\mathbf{V}_k \bar{\mathbf{p}}}{\bar{\mathbf{p}}^H \mathbf{V}_k \bar{\mathbf{p}}} \right) \\ & \left. + \frac{4\nu \log 2}{LP^2} \sum_{u=1}^L \left(\bar{\mathbf{p}}^H \mathbf{A}(\theta_u) \bar{\mathbf{p}} - \bar{\mathbf{p}}^H \mathbf{T}(\theta_u) \bar{\mathbf{p}} \right) \times \left(\mathbf{A}(\theta_u) \bar{\mathbf{p}} - \mathbf{T}(\theta_u) \bar{\mathbf{p}} \right) \right]. \end{aligned} \quad (87)$$

Therefore, equating (87) to zero and reformulating it as expressed in (66), $\mathbf{L}(\bar{\mathbf{p}}, \nu)$, $\mathbf{R}(\bar{\mathbf{p}}, \nu)$ and $\zeta(\bar{\mathbf{p}}, \nu)$ can be obtained respectively as follows.

$$\begin{aligned} \mathcal{L}(\bar{\mathbf{p}}, \nu) = & \zeta_{\text{num}}(\bar{\mathbf{p}}, \nu) \times \\ & \left[\sum_{k=1}^K \left\{ \frac{\exp \left(-\eta \frac{\bar{\mathbf{p}}^H \mathbf{U}_c(k) \bar{\mathbf{p}}}{\bar{\mathbf{p}}^H \mathbf{V}_c(k) \bar{\mathbf{p}}} \right)}{\sum_{j=1}^K \exp \left(-\eta \log_2 \frac{\bar{\mathbf{p}}^H \mathbf{U}_c(j) \bar{\mathbf{p}}}{\bar{\mathbf{p}}^H \mathbf{V}_c(j) \bar{\mathbf{p}}} \right)} \right\} \frac{\mathbf{U}_c(k)}{\bar{\mathbf{p}}^H \mathbf{U}_c(k) \bar{\mathbf{p}}} + \sum_{k=1}^K \left(\frac{\mathbf{U}_k}{\bar{\mathbf{p}}^H \mathbf{U}_k \bar{\mathbf{p}}} \right) \right. \\ & \left. + \frac{4\nu \log 2}{LP^2} \sum_{u=1}^L \left((\bar{\mathbf{p}}^H \mathbf{A}(\theta_u) \bar{\mathbf{p}}) \mathbf{A}(\theta_u) + (\bar{\mathbf{p}}^H \mathbf{T}(\theta_u) \bar{\mathbf{p}}) \mathbf{T}(\theta_u) \right) \right], \end{aligned} \quad (88)$$

$$\mathbf{R}(\bar{\mathbf{p}}, \nu) = \zeta_{\text{den}}(\bar{\mathbf{p}}, \nu) \times \left[\sum_{k=1}^K \left\{ \frac{\exp\left(-\eta \frac{\bar{\mathbf{p}}^H \mathbf{U}_c(k) \bar{\mathbf{p}}}{\bar{\mathbf{p}}^H \mathbf{V}_c(k) \bar{\mathbf{p}}}\right)}{\sum_{j=1}^K \exp\left(-\eta \log_2 \frac{\bar{\mathbf{p}}^H \mathbf{U}_c(j) \bar{\mathbf{p}}}{\bar{\mathbf{p}}^H \mathbf{V}_c(j) \bar{\mathbf{p}}}\right)} \right\} \frac{\mathbf{V}_c(k)}{\bar{\mathbf{p}}^H \mathbf{V}_c(k) \bar{\mathbf{p}}} + \sum_{k=1}^K \left(\frac{\mathbf{V}_k}{\bar{\mathbf{p}}^H \mathbf{V}_k \bar{\mathbf{p}}} \right) \right. \\ \left. + \frac{4\nu \log 2}{LP^2} \sum_{u=1}^L \left((\bar{\mathbf{p}}^H \mathbf{A}(\theta_u) \bar{\mathbf{p}}) \mathbf{T}(\theta_u) + (\bar{\mathbf{p}}^H \mathbf{T}(\theta_u) \bar{\mathbf{p}}) \mathbf{A}(\theta_u) \right) \right], \quad (89)$$

and

$$\zeta(\bar{\mathbf{p}}, \nu) = \left\{ \frac{1}{K} \sum_{k=1}^K \exp\left(-\eta \log_2 \left(\frac{\bar{\mathbf{p}}^H \mathbf{U}_c(k) \bar{\mathbf{p}}}{\bar{\mathbf{p}}^H \mathbf{V}_c(k) \bar{\mathbf{p}}} \right) \right) \right\}^{-\frac{1}{\eta \log_2 e}} \\ \times \prod_{k=1}^K \frac{\bar{\mathbf{p}}^H \mathbf{U}_k \bar{\mathbf{p}}}{\bar{\mathbf{p}}^H \mathbf{V}_k \bar{\mathbf{p}}} \times 2^{\nu \left(\frac{1}{LP^2} \sum_{u=1}^L |\bar{\mathbf{p}}^H \mathbf{A}(\theta_u) \bar{\mathbf{p}} - \bar{\mathbf{p}}^H \mathbf{T}(\theta_u) \bar{\mathbf{p}}|^2 - \frac{T_{\text{mse}}}{P^2} \right)} \quad (90)$$

$$= \frac{\zeta_{\text{num}}(\bar{\mathbf{p}}, \nu)}{\zeta_{\text{den}}(\bar{\mathbf{p}}, \nu)}. \quad (91)$$

This completes the proof.

REFERENCES

- [1] A. Liu, Z. Huang, M. Li, Y. Wan, W. Li, T. X. Han, C. Liu, R. Du, D. K. P. Tan, J. Lu, Y. Shen, F. Colone, and K. Chetty, "A survey on fundamental limits of integrated sensing and communication," *IEEE Commun. Surv. Tutor.*, vol. 24, no. 2, pp. 994–1034, 2022.
- [2] J. Choi, J. Park, N. Lee, and A. Alkhatieb, "Joint and robust beamforming framework for integrated sensing and communication systems," *IEEE Trans. Wireless Commun.*, vol. 23, no. 11, pp. 17602–17618, 2024.
- [3] X. Liu, T. Huang, N. Shlezinger, Y. Liu, J. Zhou, and Y. C. Eldar, "Joint transmit beamforming for multiuser MIMO communications and MIMO radar," *IEEE Trans. Signal Process.*, vol. 68, pp. 3929–3944, 2020.
- [4] C. Xu, B. Clerckx, S. Chen, Y. Mao, and J. Zhang, "Rate-splitting multiple access for multi-antenna joint radar and communications," *IEEE J. Sel. Topics Signal Process.*, vol. 15, no. 6, pp. 1332–1347, 2021.
- [5] Z. Wang, X. Mu, and Y. Liu, "Bidirectional integrated sensing and communication: Full-duplex or half-duplex?" *IEEE Trans. Wireless Commun.*, vol. 23, no. 8, pp. 8184–8199, Aug. 2024.
- [6] L. Liu, S. Zhang, R. Du, T. X. Han, and S. Cui, "Networked sensing in 6G cellular networks: Opportunities and challenges," *ArXiv Preprint*, 2022. [Online]. Available: <https://arxiv.org/abs/2206.00493>
- [7] Y. Zhang, Z. Gao, J. Zhao, Z. He, Y. Zhang, C. Lu, and P. Xiao, "AI empowered channel semantic acquisition for 6G integrated sensing and communication networks," *IEEE Network*, vol. 38, no. 2, pp. 45–53, 2024.
- [8] M. B. Khalilsarai, Y. Song, T. Yang, and G. Caire, "FDD massive MIMO channel training: Optimal rate-distortion bounds and the spectral efficiency of "One-Shot" schemes," *IEEE Trans. Wireless Commun.*, vol. 22, no. 9, pp. 6018–6032, 2023.
- [9] G. Y. Y. Xu and S. Mao, "User grouping for massive MIMO in FDD systems: New design methods and analysis," *IEEE Access*, vol. 2, pp. 947–959, 2014.
- [10] S.-S. Raymond, A. Abubakari, and H.-S. Jo, "Coexistence of power-controlled cellular networks with rotating radar," *IEEE J. Sel. Areas Commun.*, vol. 34, no. 10, pp. 2605–2616, 2016.
- [11] F. Liu, L. Zhou, C. Masouros, A. Li, W. Luo, and A. Petropulu, "Toward dual-functional radar-communication systems: Optimal waveform design," *IEEE Trans. Signal Process.*, vol. 66, no. 16, pp. 4264–4279, Aug. 2018.
- [12] L. Chen, F. Liu, W. Wang, and C. Masouros, "Joint radar-communication transmission: A generalized Pareto optimization framework," *IEEE Trans. Signal Process.*, vol. 69, pp. 2752–2765, 2021.
- [13] G. Caire, N. Jindal, M. Kobayashi, and N. Ravindran, "Multiuser MIMO achievable rates with downlink training and channel state feedback," *IEEE Trans. Intell. Transp. Syst.*, vol. 56, no. 6, pp. 2845–2866, 2010.
- [14] J. Park, N. Lee, J. G. Andrews, and R. W. Heath Jr., "On the optimal feedback rate in interference-limited multi-antenna cellular systems," *IEEE Trans. Wireless Commun.*, vol. 15, no. 8, pp. 5748–5762, 2016.
- [15] S. Wang, W. Dai, H. Wang, and G. Y. Li, "Robust waveform design for integrated sensing and communication," *IEEE Trans. Signal Process.*, vol. 72, pp. 3122–3138, 2024.
- [16] Z. Ren, L. Qiu, J. Xu, and D. W. K. Ng, "Robust transmit beamforming for secure integrated sensing and communication," *IEEE J. Sel. Topics Signal Process.*, vol. 71, no. 9, pp. 5549–5564, 2023.
- [17] M. Luan, B. Wang, Z. Chang, T. Hämäläinen, and F. Hu, "Robust beamforming design for ris-aided integrated sensing and communication system," *IEEE Trans. Intell. Transp. Syst.*, vol. 24, no. 6, pp. 6227–6243, 2023.
- [18] B. Ahmad and M. Chaffii, "Robust integrated sensing and communication beamforming for dual-functional radar and communications: Method and insights," *ArXiv Preprint*, 2023. [Online]. Available: <https://arxiv.org/abs/2303.07652>
- [19] D. Vasisht, B. Kumar, H. Rahul, and D. Katabi, "Eliminating channel feedback in next-generation cellular networks," in *Proc. of the ACM SIGCOMM Conf.*, 2016, pp. 398–411.
- [20] T. Choi, F. Rottenberg, J. Gómez-Ponce, A. Ramesh, P. Luo, C. J. Zhang, and A. F. Molisch, "Experimental investigation of frequency domain channel extrapolation in massive MIMO systems for zero-feedback FDD," *IEEE Trans. Wireless Commun.*, vol. 20, no. 1, pp. 710–725, 2021.
- [21] Y. Han, T. H. Hsu, C. K. Wen, K. K. Wong, and S. Jin, "Efficient downlink channel reconstruction for FDD multi-antenna systems," *IEEE Trans. Wireless Commun.*, vol. 18, no. 6, pp. 3161–3176, June 2019.
- [22] F. Rottenberg, T. Choi, P. Luo, C. J. Zhang, and A. F. Molisch, "Performance analysis of channel extrapolation in FDD massive MIMO systems," *IEEE Trans. Wireless Commun.*, vol. 19, no. 4, pp. 2728–2741, Apr. 2020.
- [23] B. Mamandipoor, D. Ramasamy, and U. Madhoo, "Newtonized orthogonal matching pursuit: Frequency estimation over the continuum," *IEEE Trans. Signal Process.*, vol. 64, no. 19, pp. 5066–5081, Oct. 2016.
- [24] N. Kim, I. P. Roberts, and J. Park, "Splitting messages in the dark—Rate-splitting multiple access for FDD massive MIMO without CSI feedback," *ArXiv Preprint*, 2024. [Online]. Available: <https://arxiv.org/abs/2405.00979>
- [25] J. Park, J. Choi, N. Lee, W. Shin, and H. V. Poor, "Rate-splitting multiple access for downlink MIMO: A generalized power iteration approach," *IEEE Trans. Wireless Commun.*, vol. 22, no. 3, pp. 1588–1603, Mar. 2023.
- [26] D. Han, J. Park, and N. Lee, "FDD massive MIMO without CSI feedback," *IEEE Trans. Wireless Commun.*, vol. 23, no. 5, pp. 4518–4530, 2024.
- [27] Z. Zhong, L. Fan, and S. Ge, "FDD massive MIMO uplink and downlink channel reciprocity properties: Full or partial reciprocity?" *Proc. IEEE Glob. Comm. Conf.*, Dec. 2020.
- [28] J. Park *et al.*, "Rate-splitting multiple access for 6G networks: Ten promising scenarios and applications," *IEEE Network*, vol. 38, no. 3, pp. 128–136, 2024.
- [29] H. Joudeh and B. Clerckx, "Sum-rate maximization for linearly precoded downlink multiuser MISO systems with partial CSIT: A rate-splitting approach," *IEEE Trans. Commun.*, vol. 64, no. 11, pp. 4847–4861, 2016.
- [30] L. Yin, Y. Mao, O. Dizdar, and B. Clerckx, "Rate-splitting multiple access for 6g—part II: Interplay with integrated sensing and communications," *IEEE Communications Letters*, vol. 26, no. 10, pp. 2237–2241, 2022.
- [31] F. Liu, Y.-F. Liu, A. Li, C. Masouros, and Y. C. Eldar, "Cramér-rao bound optimization for joint radar-communication beamforming," *IEEE Trans. Signal Process.*, vol. 70, pp. 240–253, 2022.
- [32] E. Björnson, L. Sanguinetti, and M. Debbah, "Massive MIMO with imperfect channel covariance information," in *Proc. of Asilomar Conf. on Sign., Syst. and Computers*, 2016, pp. 974–978.
- [33] S. M. Kay, "Statistical signal processing: estimation theory," *Prentice Hall*, vol. 1, pp. Chapter–3, 1993.
- [34] B. G. Lindsay and B. Li, "On second-order optimality of the observed Fisher information," *The Annals of Statistics*, vol. 25, no. 5, pp. 2172–2199, 1997.
- [35] B. Efron and D. V. Hinkley, "Assessing the accuracy of the maximum likelihood estimator: Observed versus expected fisher information," *Biometrika*, vol. 65, no. 3, pp. 457–483, 1978.
- [36] A. De Maio, S. De Nicola, Y. Huang, S. Zhang, and A. Farina, "Code design to optimize radar detection performance under accuracy and similarity constraints," *IEEE Trans. Signal Process.*, vol. 56, no. 11, pp. 5618–5629, 2008.